PERGAMON

Deep-Sea Research II 49 (2002) 2713–2745

DEEP-SEA RESEARCH
PART II

www.elsevier.com/locate/dsr2

One-dimensional ecosystem model of the equatorial Pacific upwelling system. Part I: model development and silicon and nitrogen cycle

F. Chai[a,*], R.C. Dugdale[b], T.-H. Peng[c], F.P. Wilkerson[b], R.T. Barber[d]

[a] *School of Marine Science, University of Maine, 5471 Libby Hall, Orono, ME 04469-5741, USA*
[b] *Romberg Tiburon Center, San Francisco State University, PO Box 855, Tiburon, CA 94920, USA*
[c] *NOAA Atlantic Oceanographic and Meteorological Laboratory, Ocean Chemistry Division, 4301 Rickenbacker Causeway, Miami, FL 33149-1026, USA*
[d] *Duke University, NSOE Marine Laboratory, 135 Duke Marine Lab Road, Baeufort, NC 28516, USA*

Received 20 August 2000; received in revised form 26 March 2001; accepted 10 April 2001

Abstract

A one-dimensional ecosystem model was developed for the equatorial Pacific upwelling system, and the model was used to study nitrogen and silicon cycle in the equatorial Pacific. The ecosystem model consisted of 10 components (nitrate, silicate, ammonium, small phytoplankton, diatom, micro- and meso-zooplankton, detrital nitrogen and silicon, and total CO_2). The ecosystem model was forced by the area-averaged (5°S–5°N, 90°W–180°, the Wyrtki Box) annual mean upwelling velocity and vertical diffusivity obtained from a three-dimensional circulation model. The model was capable of reproducing the low-silicate, high-nitrate, and low-chlorophyll (LSHNLC) conditions in the equatorial Pacific. The linkage to carbon cycle was through the consumption of assimilated nitrate and silicate (i.e. new productions).

Model simulations demonstrated that low-silicate concentration in the equatorial Pacific limits production of diatoms, and it resulted in low percentage of diatoms, 16%, in the total phytoplankton biomass. In the area of 5°S–5°N and 90°W–180°, the model produced an estimated sea-to-air CO_2 flux of 4.3 mol m^{-2} yr^{-1}, which is consistent with the observed results ranging of 1.0–4.5 mol m^{-2} yr^{-1}. The ammonium inhibition played an important role in determining the nitrogen cycle in the model. The modeled surface nitrate concentration could increase by a factor of 10 (from 0.8 to 8.0 mmol m^{-3}) when the strength of the ammonium inhibition increased from $\psi = 1.0$ to 10.0 (mmol m^{-3})$^{-1}$. The effects of both micro- and meso-zooplankton grazing were tested by varying the micro- and meso-zooplankton maximum grazing rates, $G1_{max}$ and $G2_{max}$. The modeled results were quite sensitive to the zooplankton grazing parameters. The current model considered the role of iron implicitly through the parameters that determine the growth rate of diatoms. Several iron-enrichment experiments were conducted by changing the parameter α (the initial slope of the photosynthetic rate over irradiance at low irradiance), $K_{Si(OH)_4}$ (half-saturation concentration of silicate uptake by diatom), and $\mu 2_{max}$ (the potential maximum specific diatom growth rate) in the regulation terms of silicate uptake by diatom. Within the first 5 days in the modeled iron-enrichment experiment, the diatom biomass increased from 0.08 to 2.5 mmol m^{-3}, more than a factor of 30 increase. But the diatom populations crashed 2 weeks after the experiment started, due to exhaustion of available silicate and increased mesozooplankton population. The modeled

*Corresponding author.
E-mail addresses: fchai@maine.edu (F. Chai), rdugdale@sfsu.edu (R.C. Dugdale), peng@aoml.noaa.gov (T.-H. Peng), fwilkers@sfsu.edu (F.P. Wilkerson), rbarber@duke.edu (R.T. Barber).

0967-0645/02/$ - see front matter
PII: S0967-0645(02)00055-3

iron-enrichment experiments produced several ecological behaviors similar to these observed during the IronEx-2.

1. Introduction

In the central and eastern equatorial Pacific Ocean, the easterly trade winds blowing along the equator create a divergence in the surface flow field that generates equatorial upwelling. The obvious manifestations of equatorial upwelling are lower sea-surface temperatures and higher concentration macronutrients, such as nitrate and phosphate. Nitrate upwelled into the euphotic zone in the equatorial Pacific region accounts for one-fifth of the estimated global upwelled nitrate (Chavez and Toggweiler, 1995). Equatorial upwelling also brings up subsurface water with relatively high concentrations of total inorganic carbon (ΣCO_2), which results in the outgassing one petagram of carbon (PgC) per year to the atmosphere (Feely et al., 1997), making the equatorial Pacific the largest natural source of CO_2 to the atmosphere, and contributing about 70% of interannual variability of atmospheric pCO_2.

The importance of the equatorial Pacific Ocean in global biogeochemical fluxes was recognized by earlier studies (Chavez and Barber, 1987; Feely et al., 1997). Yet along with a rather clear understanding of the basic upwelling character of the eastern and central equatorial Pacific, there remains an equatorial enigma: relatively low phytoplankton biomass persists despite relatively high concentrations of inorganic nutrients (nitrate and phosphate) in the euphotic zone, abundant light, and the absence of deep mixing. This high-nutrient, low-chlorophyll (HNLC) condition has puzzled equatorial oceanographers for decades (Barber and Ryther, 1969; Walsh, 1976; Thomas, 1972; Barber, 1992; Minas and Minas, 1992). The lack of correlation in the zonal dimension between macronutrient concentrations (especially in the zonal dimension) and phytoplankton productivity, biomass or chlorophyll-specific productivity rates has been well documented (Barber and Chavez, 1991).

Current explanations of the equatorial enigma are to suggest the iron limitation of phytoplankton productivity combined with microzooplankton grazing control (Landry et al., 1997), or to consider silicate limitation on diatom growth (Dugdale and Wilkerson, 1998). Diatoms appear to dominate new and export production during strong upwelling period, which creates higher vertical flux of silicate and iron to the euphotic zone (Dunne et al., 1999). In the equatorial Pacific, as in oligotrophic oceanic regions, pico- and nanophytoplankton dominate the phytoplankton community (Bidigare and Ondrusek, 1996). Fueled with regenerated nitrogen and iron, the specific growth and productivity rates of these small phytoplankton are relatively high, but microzooplankton grazing removes most of the accumulated biomass each day (Landry et al., 1995; Verity et al., 1996). In two equatorial Pacific iron addition experiments, which highlighted the important role of iron in equatorial HNLC waters, all of the ambient phytoplankton, including pico- and nanophytoplankton, had significantly increased productivity (Martin et al., 1994; Coale et al., 1996) following the addition of iron. In the second experiment, which involved multiple iron additions, phytoplankton composition was altered by a massive accumulation (to about 2.4 mg Chl m^{-3}) of large diatoms (Coale et al., 1996). It was the accumulation of a high biomass bloom of these large ($>5\,\mu m$), potentially fast-sinking phytoplankton in IronEx-2 that drew down the mixed-layer pCO_2. Such high biomass blooms, if they are efficiently exported below the mixed layer, have the potential to alter ocean-atmosphere partitioning of carbon.

It is also clear that silicic acid concentration, as well as iron, regulates diatom growth and biomass accumulation in equatorial HNLC waters (Ku et al., 1995; Dugdale and Wilkerson, 1998). When the supply of silicon and iron to the euphotic zone is enhanced by relatively cool (quasi La Niña) conditions (Barber et al., 1996), tropical instability waves (TIWs) (Foley et al., 1997) or strong frontal upwelling, diatoms $>5\,\mu m$ increase in both absolute and proportional abundance. Dunne et al. (1999) found that diatoms

dominated the material collected by sediment traps in these natural enrichment events. However, in these events diatoms never dominated the water-column phytoplankton assemblage; at most about 20–25% of the chlorophyll present in the water column was diatom chlorophyll (Bidigare and Ondrusek, 1996). In contrast, in the IronEx-2 experiment >80% of the chlorophyll was diatom chlorophyll associated with cells >5 μm.

Recently available observations, better understanding, and new hypotheses on the regulation of equatorial Pacific productivity and biomass make this a productive time to model the biogeochemical processes involving iron, nitrogen and silicon and their linkage to the carbon cycle in the equatorial Pacific. Earlier ecosystem model studies of the equatorial Pacific Ocean by Toggweiler and Carson (1995) and Chai et al. (1996) used a three-dimensional general circulation model and a simplified nitrogen-based ecosystem model with five components to investigate the equatorial nitrate budget. Loukos et al. (1997) incorporated iron limitation into a nitrogen-based, one-dimensional ecosystem model for 140°W and the equator. These three early model studies had only one phytoplankton size class and one zooplankton size class. Leonard et al. (1999) expanded a one-dimensional iron and nitrogen-based model to include two phytoplankton size classes and two zooplankton size classes, and used this one-dimensional 9-component ecosystem model to study the biological response to El Niño variability. Friedrichs and Hofmann (2001) used physical observations from the Tropical Atmosphere Ocean (TAO) mooring array to force a 5-component nitrogen-based ecosystem model calibrated for 140°W on the equator. With this model they investigated the biological responses to physical variability on time scales ranging from daily to interannual. All three of the one-dimensional, 140°W equatorial models (Loukos et al., 1997; Leonard et al., 1999; and Friedrichs and Hofmann, 2001) included iron limitation of phytoplankton growth, but none included silicon limitation of diatom growth and accumulation.

Combining a nitrogen-based ecosystem model (Chai et al., 1996) with a silicon limitation model (Dugdale and Wilkerson, 1998), we developed a realistic ecosystem model with iron limitation included implicitly through the initial slopes (alpha) of the P vs. E relationship (Chai et al., 2000; Lindley and Barber, 1998). The one-dimensional upper-ocean ecosystem model study described here was forced with the physical processes in the equatorial Pacific and shows how physical variability affects a food web with both large (>5 μm) and small (<5 μm) phytoplankton size classes as well as both micro- and mesozooplankton grazers. This report describes the model used in this study, presents the ecosystem model equations, and discusses the linkage of the food web dynamics to the carbon chemistry in the equatorial upper ocean.

2. Model description

2.1. The model

The horizontal coverage of the model is 5°S–5°N and 90°W–180°, defined as the Wyrtki Box. Based upon surface air-to-sea heat flux in this region, Wyrtki (1981) estimated, on average, that about 50 Sv of cold water upwelled across 100 m depth. The effects of horizontal advection are minimized using this approach, when comparing with models only focused at one fixed point. The vertical domain of the ecosystem model is from the ocean surface down to 200 m. There are 33 levels in the vertical, which provides a resolution of 5 m within the upper 120 and 10 m resolution between 120 and 200 m. The inputs of the physical forcing are the area-averaged (over the Wyrtki Box) annual mean upwelling velocity and vertical diffusivity (Fig. 1), which are obtained from the simulations of the three-dimensional ocean circulation model for the equatorial Pacific (see Chai et al., 1996 for details). The model also includes both temperature and salinity as two state variables. By doing so, the modeled sea-surface temperature (SST) and the air-to-sea heat flux are compared with observations, and such comparisons are served as the criteria on validating the modeled

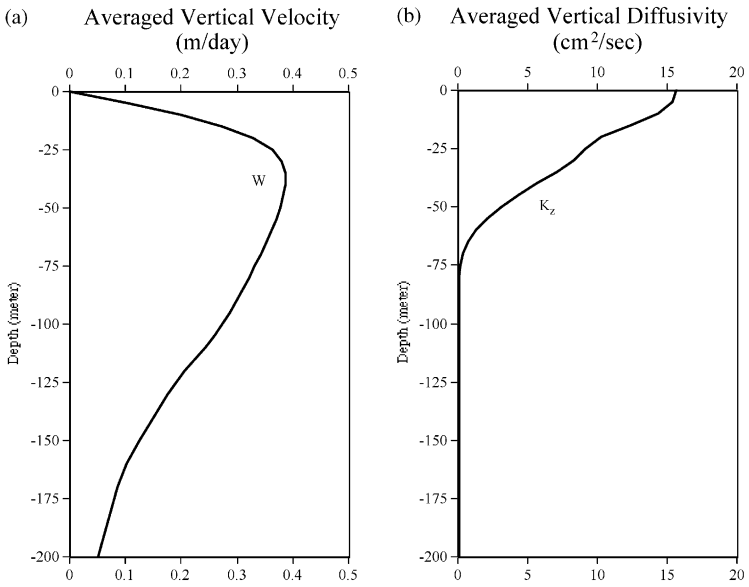

Fig. 1. (a) The area-averaged (5°S–5°N, 90°W–180°) annual mean vertical velocity ($m\,day^{-1}$) from the ocean general circulation model (Chai et al., 1996); (b) The area-averaged (5°S–5°N, 90°W–180°) annual mean vertical diffusivity ($cm^2\,s^{-1}$) based upon the formulation by Pacanowski and Philander (1981).

upwelling velocity and vertical diffusivity. For example, if the modeled SST is too low and the heat flux from the atmosphere to the ocean is too high, which indicate the upwelling velocity used in this simulation is too strong, then the upwelling rates need to be reduced. In general, the SST is between 25°C and 26°C and the heat flux is about $100\,W/m^2$ in the Wyrtki Box.

The ecosystem model is adopted from original 5-component structure of Chai et al. (1996) by modulating impact of silicate limitation on diatom production. The current model has ten components representing two sizes of phytoplankton, small phytoplankton cells (S1) ($<5\,\mu m$ in diameter) and diatoms (S2), micro- and meso-zooplankton (Z1 and Z2), non-living detrital nitrogen and silicate (DN and DSi), dissolved silicic acid (silicate; $(SiOH)_4$), and two forms of dissolved inorganic nitrogen: nitrate and ammonium (NO_3 and NH_4), total CO_2 (TCO_2). The inter-compartmental flows of this ecosystem are shown in Fig. 2.

S1 represents small, easily grazed phytoplankton whose specific growth varies, but whose biomass is regulated by micrograzers (Z1) and whose daily net productivity is largely remineralized (Chavez et al., 1991; Frost, 1991; Murray et al., 1994; Landry et al., 1995, 1997). S2 represents relatively large phytoplankton ($>5\,\mu m$ in diameter) that makes up high biomass blooms and contributes disproportionately to sinking flux as ungrazed production or large fecal pellets (Smetacek, 1985; Wefer, 1989; Peinert et al., 1989; Bidigare and Ondrusek, 1996). The S2 phytoplankton class has the potential to grow fast under optimal nutrient conditions (N, Si, and Fe concentrations $\gg K_S$, Michaelis–Menten constant for nutrient uptake) (Frost, 1996; Coale et al., 1996). Z1 represents small micrograzers whose specific growth rate are similar to S1 phytoplankton, and whose grazing rate is density-dependent (Landry et al., 1997). Z2 represents larger mesozooplankton that graze on S2 and detritus nitrogen (DN) and prey on Z1. The Z2 zooplankton have a feeding threshold with conventional grazing dynamics as described in Frost and Franzen (1992). The detrital pool is split into detrital nitrogen (DN) and silicon (DSi) in order to balance supplies of nitrogen and silicon through the upwelling and vertical mixing separately. The detrital silicon (DSi) sinks faster than the detrital nitrogen (DN).

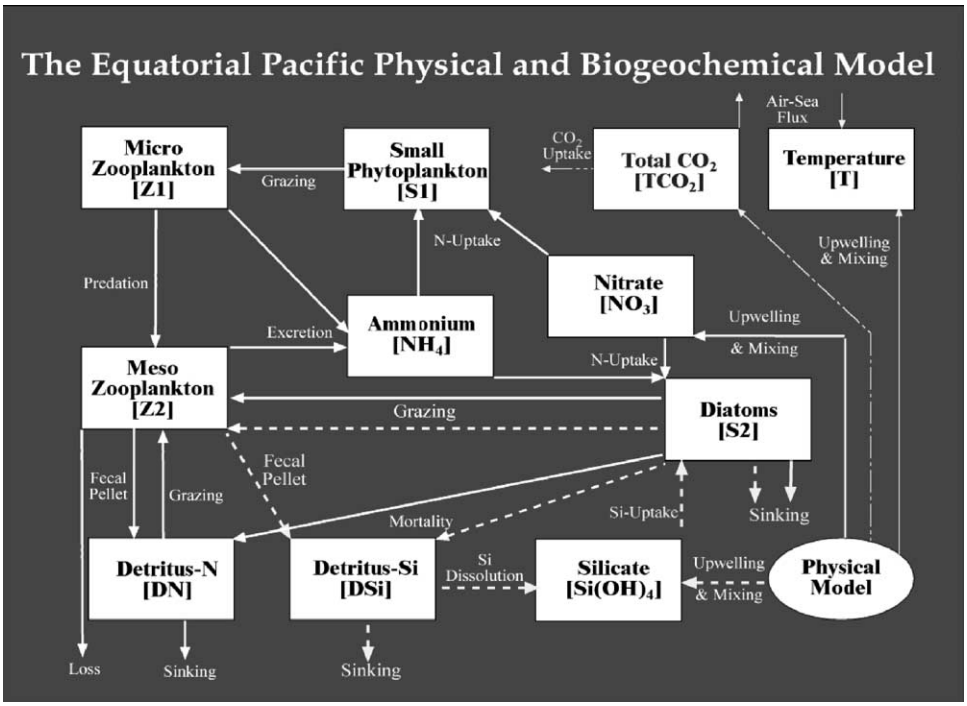

Fig. 2. The inter-compartmental flow chart of the ecosystem and linkage to carbon and physical processes. The flow of nitrogen is indicated by solid line; the flow of silicon is indicated by dashed line; and the carbon flow is indicated by line-dashed line.

2.2. The equations

The model equations describing each compartment all take the form

$$\frac{\partial C_i}{\partial t} = \mathrm{PHYSICS}(C_i) + \mathrm{BIOLOGY}(C_i) \quad i = 1, \ldots, 9. \tag{1}$$

(For example, $C_1 = NO_3$, $C_2 = NH_4$, and so on). The term PHYSICS(C_i) represents the contribution to the concentration change due to physical processes, including vertical advection and eddy diffusion.

$$\mathrm{PHYSICS}(C_i) = \underbrace{-w\frac{\partial C_i}{\partial z}}_{\text{advection}} \quad \underbrace{+\frac{\partial}{\partial z}\left(A_{\mathrm{Tv}}\frac{\partial C_i}{\partial z}\right)}_{\text{eddy diffusivity}} \tag{2}$$

Here w is vertical velocity, and A_{Tv} is vertical eddy diffusion coefficient. The values for w and A_{Tv} are showed in Fig. 1. The annual mean upwelling velocity and vertical diffusivity are the area-averaged (over the Wyrtki Box), which are obtained from the simulations of the three-dimensional ocean circulation model for the equatorial Pacific (Chai et al., 1996). The upwelling velocity and vertical diffusivity do not change with time, so only the steady state simulations are conducted with this one-dimensional model.

The term BIOLOGY(C_i) represents biological sources and sinks of that compartment. In the euphotic zone (the upper 120 m), the biological terms, BIOLOGY(C_i), are:

$$\mathrm{BIOLOGY}(NO_3) = \underbrace{-\mathrm{NPS1}}_{NO_3\text{ uptake by S1}} \quad \underbrace{-(\mathrm{NPS2} - \mathrm{RPS2})}_{NO_3\text{ uptake by S2}} \tag{3}$$

Note: Nitrate is used by both small phytoplankton (S1) and diatoms (S2). The total nitrogen requirement for diatoms are from two parts, NH_4 and NO_3. NH_4 uptake by diatoms, RPS2, is calculated directly (see Eq. (17)). Assuming the Si/N uptake ratio by diatoms is one, then the rest nitrogen required by diatoms is from nitrate pool, which is: NPS2–RPS2. NPS2 is silicate uptake by diatoms, see Eq. (16).

$$\underset{}{\text{BIOLOGY}(\text{Si(OH)}_4) =} \underbrace{-\text{NPS2}}_{\text{Si(OH)}_4\text{ uptake by S2}} \underbrace{+\gamma_4\text{DSI}}_{\text{Si dissolution from DSI}} \tag{4}$$

$$\underset{}{\text{BIOLOGY}(\text{NH}_4) =} \underbrace{-\text{RPS1}}_{\text{NH}_4\text{ uptake by S1}} \underbrace{-\text{RPS2}}_{\text{NH}_4\text{ uptake by S2}} \underbrace{+\text{reg}_1 Z1 + \text{reg}_2 Z2}_{\text{NH}_4\text{ regeneration}} \tag{5}$$

$\text{reg}_1 = 0.2\,\text{day}^{-1}$ (microzooplankton excretion rate of ammonium),
$\text{reg}_2 = 0.1\,\text{day}^{-1}$ (mesozooplankton excretion rate of ammonium),

$$\underset{}{\text{BIOLOGY}(\text{S1}) =} \underbrace{+(\text{NPS1} + \text{RPS1})}_{\text{total production by S1}} \underbrace{-G_1}_{\text{grazing by Z1}} \tag{6}$$

$$\underset{}{\text{BIOLOGY}(\text{S2}) =} \underbrace{+2\text{NPS2}}_{\text{production by S2}} \underbrace{-2G_2}_{\text{grazing by Z2}} \underbrace{-2\frac{\partial}{\partial z}(w_1\text{S2})}_{\text{sinking}} \underbrace{-2\gamma_3\text{S2}}_{\text{mortality}} \tag{7}$$

$w_1 = 1.0\,\text{m day}^{-1}$ (diatoms sinking speed),
$\gamma_3 = 0.05\,\text{day}^{-1}$ (diatom specific mortality rate).

Note: all the source and sink terms are counted twice for diatom growth in order to reflect both nitrogen and silicon uptake by diatoms, silicon to nitrogen ratio is 1:1 in diatoms (Brzezinski, 1985), the uptake silicon to nitrogen ratio by diatoms is also 1 (Leynaert et al., 2001). We do not allow silicon to nitrogen ratio in diatoms change in the current model. Some recent studies by Takeda (1998) suggested that silicon to nitrogen uptake ratio by diatoms varies by about a factor of 4, depending upon ambient iron concentrations, but processes contribute such variation are still not clear.

$$\underset{}{\text{BIOLOGY}(\text{Z1}) =} \underbrace{+G_1}_{\text{grazing on S1}} \underbrace{-G_3}_{\text{predation by Z2}} \underbrace{-\text{reg}_1\text{Z1}}_{\text{NH}_4\text{ reg}} \tag{8}$$

$$\underset{}{\text{BIOLOGY}(\text{Z2}) =} \underbrace{(G_2 + G_3 + G_4)}_{\text{grazing by Z2}} \underbrace{-(1-\gamma_1)(G_2 + G_3 + G_4)}_{\text{detritus-N prod.}} \underbrace{-\text{reg}_2\text{Z2}}_{\text{NH}_4\text{ reg.}} \underbrace{-\gamma_2\text{Z2}^2}_{\text{Loss}} \tag{9}$$

$\gamma_1 = 0.75$ (mesozooplankton assimilation efficiency on Z1 and DN),
$\gamma_2 = 0.05\,(\text{mmol m}^{-3})^{-1}\,\text{day}^{-1}$ (mesozooplankton specific mortality rate).

Note: the fecal pellet production of silicate by Z2 equals to the grazing on diatoms by Z2, which is G_2, two terms cancel each other in the Eq. (9). In this sense, the Z2 component just passes the silicate from the diatoms directly to the detritus-Si pool. G_3 is predation term on Z1 by Z2. G_4 is grazing term on DN by Z2.

$$\underset{}{\text{BIOLOGY}(\text{DN}) =} \underbrace{+(1-\gamma_1)(G_2 + G_3 + G_4)}_{\text{detritus-N prod.}} \underbrace{-G_4}_{\text{grazing by Z2}} \underbrace{-\partial(w_2\,\text{DN})/\partial z}_{\text{sinking}} \underbrace{+\gamma_3\text{S2}}_{\text{S2 mortality}} \tag{10}$$

$w_2 = 10.0\,\text{m day}^{-1}$ (detritus nitrogen sinking speed).

$$\underset{}{\text{BIOLOGY}(\text{DSI}) =} \underbrace{+G_2}_{\text{detritus-si prod.}} \underbrace{-\partial(w_3\,\text{DSI})/\partial z}_{\text{sinking}} \underbrace{-\gamma_4\text{DSI}}_{\text{Si dissolution}} \underbrace{+\gamma_3\text{S2}}_{\text{S2 mortality}} \tag{11}$$

$w_3 = 2.0 \times w_2 = 20.0\,\text{m day}^{-1}$ (detritus silicon sinking speed).

Growth (NPS1, RPS1, NPS2, and RPS2) and grazing (G_1, G_2, G_3, and G_4) functions are expressed next, along with the values for each parameters used in the calculations. NPS1 is the nitrate-uptake rate by small phytoplankton

$$\underset{\text{NO}_3\text{ uptake by S1}}{\text{NPS1} = \mu 1_{\max}} \quad \underbrace{\frac{\text{NO}_3}{K_{\text{NO}_3} + \text{NO}_3}}_{\text{NO}_3\text{ regulation}} \quad \underbrace{\text{e}^{-\psi \text{NH}_4}}_{\text{NH}_4\text{ inhibition}} \quad \underbrace{(1 - \text{e}^{-(a/\mu 1_{\max})I})\text{S1}}_{\text{light regulation}} \tag{12}$$

$\mu 1_{\max} = 2.0\,\text{day}^{-1}$ (maximum specific growth rate of small phytoplankton),
$\psi = 5.59\ (\text{mmol m}^{-3})^{-1}$ (ammonium inhibition parameter),
$K_{\text{NO}_3} = 0.5\,\text{mmol m}^{-3}$ (half-saturation for nitrate uptake by S1).
$\alpha = 0.025\,(\text{W/m}^2)^{-1}\,\text{day}^{-1}$ (initial slope of $P-I$ curve),
I is the irradiance, and is given by

$$I(z,t) = I_0(t)\text{e}^{-k_1 z - k_2 \int_{-z}^{0} (\text{S1}+\text{S2})\,\text{d}z} \tag{13}$$

$k_1 = 0.046\,\text{m}^{-1}$ (light attenuation due to water),
$k_2 = 0.03\,\text{m}^{-1}\ (\text{mmol m}^{-3})^{-1}$ (light attenuation by small phytoplankton and diatoms), $I_0(t)$ is the surface irradiance, and during a 24 h period, takes the form:

$$I_0(t) = \begin{cases} I_0^{\text{Noon}} \sin\left(\dfrac{t-6}{12}\pi\right) & \text{(from 6 am to 6 pm)}, \\ 0 & \text{(from 6 pm to 6 am)}, \end{cases} \tag{14}$$

$I_0^{\text{Noon}} = 410\,\text{W/m}^2$ (annual noontime averaged surface irradiance, Chavez et al., 1996).
RPS1 is the ammonium uptake rate by small phytoplankton

$$\underset{\text{NH}_4\text{ uptake by S1}}{\text{RPS1} = \mu 1_{\max}} \quad \underbrace{\frac{\text{NH}_4}{K_{\text{NH}_4} + \text{NH}_4}}_{\text{NH}_4\text{ regulation}} \quad \underbrace{(1 - \text{e}^{-(a/\mu 1_{\max})I})\text{S1}}_{\text{light regulation}} \tag{15}$$

$K_{\text{NH}_4} = 0.05\,\text{mmol m}^{-3}$ (half-saturation for ammonium uptake by S1).
NPS2 is the silicate uptake rate by diatoms

$$\underset{\text{silicate uptake by S2}}{\text{NPS2} = \mu 2_{\max}} \quad \underbrace{\frac{\text{Si(OH)}_4}{K_{\text{Si(OH)}_4} + \text{Si(OH)}_4}}_{\text{Si(OH)}_4\text{ regulation}} \quad \underbrace{(1 - \text{e}^{-(a/\mu 2_{\max})I})\text{S2}}_{\text{light regulation}} \tag{16}$$

$\mu 2_{\max} = 3.0\,\text{day}^{-1}$ (the potential maximum specific diatom growth rate),
$K_{\text{si(OH)}_4} = 3.0\,\text{mmol m}^{-3}$ (half-saturation for Si(OH)_4 uptake by S2).
RPS2 is the ammonium uptake rate by diatoms:

$$\underset{\text{NH}_4\text{ uptake by S2}}{\text{RPS2} = \mu 2_{\max}} \quad \underbrace{\frac{\text{NH}_4}{K_{\text{S2}-\text{NH}_4} + \text{NH}_4}}_{\text{NH}_4\text{ regulation}} \quad \underbrace{(1 - \text{e}^{-(a/\mu 2_{\max})I})\text{S2}}_{\text{light regulation}} \tag{17}$$

$K_{\text{S2}-\text{NH}_4} = 1.0\,\text{mmol m}^{-3}$ (half-saturation for ammonium uptake by diatoms).

Note: (1) The current model allows NH_4 uptake (RPS1 and RPS2) taking place during the night, which has been suggested by some limited field and laboratory measurements (Dugdale and Goering, 1967; Cuhel et al., 1984). The light used for the NH_4 uptake during the night (6 PM to 6 AM) is half of the daily averaged light intensity. (2) The total nitrogen demand by diatoms equals to the total uptake of silicate to make up nitrogen to silicate ratio is 1:1 in diatoms (Brzezinski, 1985). There are two nitrogen sources for

diatoms required nitrogen, NH_4 and NO_3. The model calculates NH_4 uptake by diatoms (RPS2) first, and the rest of nitrogen comes from NO_3 (NPS2–RPS2), see Eq. (3).

G_1 is the microzooplankton grazing rate on small phytoplankton

$$G_1 = \mathrm{G1}_{\max} \underbrace{\frac{\mathrm{S1}}{\mathrm{K1}_{\mathrm{gr}} + \mathrm{S1}}}_{\text{food limitation}} \underbrace{\frac{\mathrm{S1}}{\mathrm{S1}_{\mathrm{ave}}}}_{\text{depth modification}} \mathrm{Z1} \tag{18}$$

$\mathrm{G1}_{\max} = 1.35\,\mathrm{day}^{-1}$ (microzooplankton maximum growth rate),
$\mathrm{K1}_{\mathrm{gr}} = 0.5\,\mathrm{mmol\,m}^{-3}$ (half-saturation for microzooplankton ingestion).
$\mathrm{S1}_{\mathrm{ave}}$ is depth averaged (within the euphotic zone) small phytoplankton, which is defined as

$$\mathrm{S1}_{\mathrm{ave}} = \frac{1}{Z'} \int_{-z'}^{0} S1 \, \mathrm{d}z. \tag{19}$$

We have found that the predator-prey oscillation could be reduced significantly in the model by modifying the grazing functions with terms $\mathrm{S1}/\mathrm{S1}_{\mathrm{ave}}$. The z' is the depth of euphotic zone, and is set to 120 m in the model.

G_2, G_3, and G_4 are the mesozooplankton grazing rates on diatoms, microzooplankton, and detrital nitrogen, respectively:

$$G_2 = \mathrm{G2}_{\max} \frac{\zeta_1 \mathrm{S2}}{\mathrm{K2}_{\mathrm{gr}} + \zeta_1 \mathrm{S2} + \zeta_2 \mathrm{Z1} + \zeta_3 \mathrm{DN}} \mathrm{Z2} \tag{20}$$

$$G_3 = \mathrm{G2}_{\max} \frac{\zeta_1 \mathrm{Z1}}{\mathrm{K2}_{\mathrm{gr}} + \zeta_1 \mathrm{S2} + \zeta_2 \mathrm{Z1} + \zeta_3 \mathrm{DN}} \mathrm{Z2} \tag{21}$$

$$G_4 = \mathrm{G2}_{\max} \frac{\zeta_1 \mathrm{DN}}{\mathrm{K2}_{\mathrm{gr}} + \zeta_1 \mathrm{S2} + \zeta_2 \mathrm{Z1} + \zeta_3 \mathrm{DN}} \mathrm{Z2} \tag{22}$$

$\mathrm{G2}_{\max} = 0.53\,\mathrm{day}^{-1}$ (mesozooplankton maximum growth rate),
$\mathrm{K2}_{\mathrm{gr}} = 0.25\,\mathrm{mmol\,m}^{-3}$ (half-saturation for mesozooplankton ingestion),
where ζ_1, ζ_2, and ζ_3 are the preferences for a given food type, and defined as following:

$$\begin{aligned} \zeta_1 &= \frac{\rho_1 \mathrm{S1}}{\rho_1 \mathrm{S1} + \rho_2 \mathrm{Z1} + \rho_3 \mathrm{DN}} \\ \zeta_2 &= \frac{\rho_2 \mathrm{Z1}}{\rho_1 \mathrm{S1} + \rho_2 \mathrm{Z1} + \rho_3 \mathrm{DN}} \\ \zeta_3 &= \frac{\rho_3 \mathrm{DN}}{\rho_1 \mathrm{S1} + \rho_2 \mathrm{Z1} + \rho_3 \mathrm{DN}} \end{aligned} \tag{23}$$

$$\rho_1 = 0.70, \quad \rho_2 = 0.20, \quad \rho_3 = 0.10.$$

Parameters used and their sources in the standard experiment are given in Table 1. Selection of the parameters is primarily based upon four major sources: (1) papers by Fasham et al. (1990), Sarmiento et al. (1993), and Chai et al. (1996); (2) observational data in the equatorial Pacific (Dugdale and Goering, 1967; Dugdale et al., 1992; Barber and Chavez, 1991; Minas et al., 1986; Peña et al., 1990); (3) data from the 1992 EqPac cruises (Barber et al., 1996; Lindley et al., 1995; Landry et al., 1995; Murray et al., 1994); and (4) historical literature.

Table 1
The model parameters

Parameters	Symbol	Value	Unit	Source
Averaged surface noontime irradiance	I_0^{Noon}	410	$\mathrm{W\,m^{-2}}$	(9)
Light attenuation due to water	k_1	0.046	$\mathrm{m^{-1}}$	(3, 5)
Light attenuation by phytoplankton	k_2	0.03	$\mathrm{m^{-1}\,(mmol\,m^{-3})^{-1}}$	(3, 5)
Initial slope of $P-I$ curve	α	0.025	$\mathrm{day^{-1}\,(W/m2)^{-1}}$	(2)
Maximum specific growth rate of small phytoplankton	$\mu 1_{\max}$	2.0	$\mathrm{day^{-1}}$	(1, 2)
Ammonium inhibition parameter	ψ	5.59	$\mathrm{(mmol\,m^{-3})^{-1}}$	(4)
Half-saturation for nitrate uptake	$K_{\mathrm{NO_3}}$	0.5	$\mathrm{mmol\,m^{-3}}$	(8)
Half-saturation for ammonium uptake by small phytoplankton	$K_{\mathrm{NH_4}}$	0.05	$\mathrm{mmol\,m^{-3}}$	(6)
Maximum specific diatom growth rate	$\mu 2_{\max}$	3.0	$\mathrm{day^{-1}}$	This study
Half-saturation for silicate uptake	$K_{\mathrm{Si(OH)_4}}$	3.0	$\mathrm{mmol\,m^{-3}}$	(12)
Half-saturation for ammonium uptake by diatoms	$K_{\mathrm{S2-NH_4}}$	1.0	$\mathrm{mmol\,m^{-3}}$	This study
Diatoms sinking speed	W_1	1.0	$\mathrm{m\,day^{-3}}$	(7)
Microzooplankton maximum grazing rate	$\mathrm{G1_{max}}$	1.35	$\mathrm{day^{-3}}$	(10)
Half-saturation for microzooplankton ingestion	$K1_{\mathrm{gr}}$	0.5	$\mathrm{mmol\,m^{-3}}$	(11)
Microzooplankton excretion rate to ammonium	$\mathrm{reg_1}$	0.2	$\mathrm{day^{-1}}$	(11)
Mesozooplankton maximum grazing rate	$\mathrm{G2_{max}}$	0.53	$\mathrm{day^{-1}}$	This study
Mesozooplankton Assimilation efficiency	γ_1	0.75		(6)
Half-saturation for mesozooplankton ingestion	$K2_{\mathrm{gr}}$	0.25	$\mathrm{mmol\,m^{-3}}$	This study
Diatom specific mortality rate	γ_3	0.05	$\mathrm{day^{-1}}$	This study
Biogenic silica dissolution rate	γ_4	0.0	$\mathrm{day^{-1}}$	This study
Mesozooplankton specific mortality rate	γ_2	0.05	$\mathrm{day^{-1}}$	(6)
Mesozooplankton excretion rate to ammonium	$\mathrm{reg_2}$	0.1	$\mathrm{day^{-1}}$	(6)
Grazing preference for diatoms	ρ_1	0.7		This study
Grazing preference for microzooplankton	ρ_2	0.2		This study
Grazing preference for detritus	ρ_3	0.1		This study
Detritus sinking speed	W_2	10.0	$\mathrm{m\,day^{-1}}$	(11)

Sources noted here are: (1) Barber and Chavez (1991); (2) Lindley et al. (1995); (3) Evans and Parslow (1985); (4) Hoffmann and Ambler (1988); (5) Fasham et al. (1990); (6) Fasham (1995); (7) Jamart et al. (1977); (8) Eppley et al. (1992); (9) Chavez et al. (1996); (10) Landry et al. (1995); (11) Sarmiento et al. (1993); (12) Dugdale and Wilkerson (1998).

2.3. The linkage to the carbon cycle

The linkage of the carbon cycle to this ecosystem model is through the consumption and remineralization of assimilated nutrients based upon the nitrogen changes in the water column by using Redfield stoichiometric ratios. The *C*/*N* ratio of 117/16 (= 7.3) of Anderson and Sarmiento (1994) is used. The total dissolved inorganic carbon ($\mathrm{TCO_2}$) is initiated with the mean value for the region of $2250\,\mu\mathrm{mol\,kg^{-1}}$ (Wanninkhof et al., 1995). To estimate the CO_2 gas exchange flux across the sea–air interface, the partial pressure of CO_2 in the surface water had to be determined. Based on the thermodynamics of carbon chemistry, the CO_2 partial pressure can be determined by the $\mathrm{TCO_2}$ and total alkalinity (TA) concentrations. Instead of modeling the distribution of alkalinity in the water column, the alkalinity of the surface box is determined only by a statistical regional representation of salinity normalized alkalinity for the equatorial Pacific Ocean with surface water temperature between 20°C and 29°C (Millero et al., 1998). The distribution of $\mathrm{TCO_2}$ in the water column can be given as

$$\begin{aligned}\partial(\mathrm{TCO_2})/\partial t = {} & \mathrm{PHYSICS(TCO_2)} \\ & + \mathrm{BIOLOGY(TCO_2)} \\ & + \mathrm{EVASION(TCO_2)}\end{aligned} \tag{24}$$

where PHYSICS(TCO_2) includes all mixing processes, BIOLOGY(TCO_2) is determined by the total phytoplankton uptake of NO_3 and $Si(OH)_4$ in each layer and the corresponding changes in TCO_2 through Redfield C/N ratio, i.e. BIOLOGY(TCO_2) = 7.3(NPS1 + NPS2). EVASION(TCO_2) is determined by the equation

$$\text{EVATION(DIC)} = E\Delta pCO_2, \tag{25}$$

where E is the mean CO_2 exchange flux of $20\,\text{mol}\,\text{m}^{-2}\,\text{yr}^{-1}$ at pCO_2 of 280 ppm, and ΔpCO_2 is the difference in partial pressure of CO_2 between surface water and atmosphere. To simulate the carbon cycle in 1992, the atmospheric pCO_2 is assumed to be constant at 357 ppm. In the equatorial Pacific, the surface water pCO_2 is higher than the atmospheric pCO_2 and hence the evasion of CO_2 from the ocean into the atmosphere. The EVASION(TCO_2) term is only applied to the surface level, and is equal to zero in the water column below surface level.

2.4. The model experiment design

There are 33 levels in the vertical, which provides a resolution of 5 m within the upper 120 and 10 m resolution between 120 and 200 m. The time interval is 1 h. The model resolves the day-and-night cycle, i.e. no nitrate and silicate uptake takes place during the night, but the model allows NH_4 uptake by both S1 and S2 during the night. The initial conditions are the area-averaged (i.e. the Wyrtki Box) observed temperature, salinity, NO_3, and $Si(OH)_4$ (Levitus et al., 1993), and observed TCO_2 (JGOFS EqPac data, http://www1.whoi.edu/mzweb/eqpac.htm). The initial conditions for all other variables are assigned with a value of $0.01\,\text{mmol}\,\text{m}^{-3}$. Below the euphotic zone (>120 m), NO_3, $Si(OH)_4$, and TCO_2 are restored back to their initial conditions, respectively. By doing so, we avoid having to model the nutrient regeneration processes directly. By using the constant vertical velocity and diffusivity, represent the annual mean conditions, the model needs to run up to 1000 days to reach the steady state for all the variables (Fig. 3). The biological variables, S1 and S2 reach steady state very fast, <200 days, whereas the temperature (T), NO_3 and $Si(OH)_4$ take much longer time to adjust (Fig. 3a–c). At the steady state, the modeled SST is 25.37°C and the air-to-sea heat flux is $104\,\text{W}/\text{m}^2$, which agree with observations (Wyrtki, 1981). This suggests that the vertical velocity and diffusivity used in the model represent the mean conditions for the region. We analyze the ecosystem model results at 1000 days, the end of the model runs.

3. Results and discussion

3.1. Vertical profiles

At the steady state, the modeled vertical profiles of NO_3, $Si(OH)_4$, and NH_4 are shown in Fig. 4. The model reproduced the low-silicate concentration than nitrate concentration between the surface and 120 m seen from real data. At 120 m, $Si(OH)_4$ concentration is $7.5\,\text{mmol}\,\text{m}^{-3}$, whereas NO_3 concentration is $12.0\,\text{mmol}\,\text{m}^{-3}$, and these values are close to the observed climatological data, respectively (Levitus et al., 1993). The depth scale of regeneration of NO_3 is much shallower than that for $Si(OH)_4$, and it results in higher NO_3 concentrations than $Si(OH)_4$ between 100 and 400 m in the observed data (Murray et al., 1995). High source NO_3 concentration and low uptake rate of NO_3 by the small phytoplankton create higher NO_3 concentrations than $Si(OH)_4$ concentrations throughout the euphotic zone. The modeled NH_4 concentration is low near the surface and reaches the maximum value at 70 m, which agrees well with the observations (Murray et al., 1995). The subsurface NH_4 maximum is due to

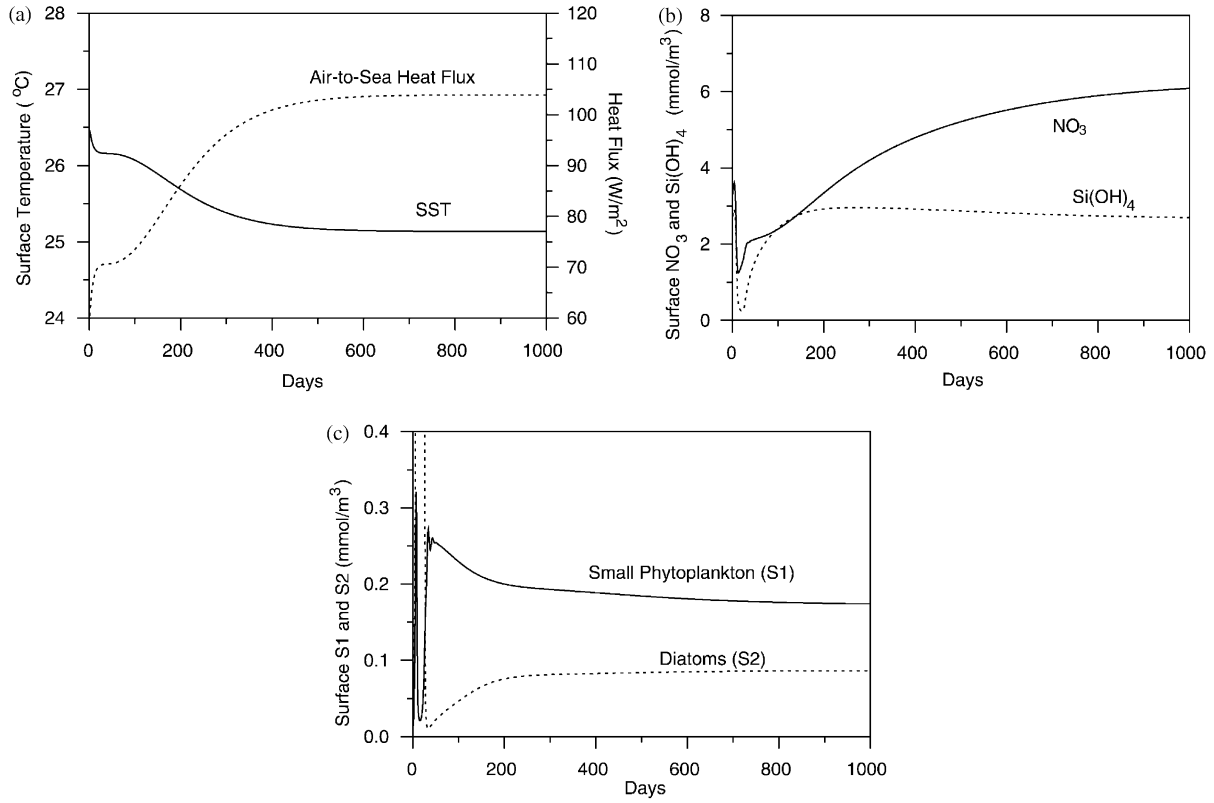

Fig. 3. Model adjustment of surface response during a 1000-day simulation: (a) SST (°C) and air-to-sea heat flux (W/m^2); (b) NO_3 and $Si(OH)_4$ concentration (mmol m^{-3}); (c) small phytoplankton and diatoms concentration (mmol m^{-3}). Most of modeled variables reach the equilibrium state after 400 days integration except NO_3. At day 1000, NO_3 is at the quasi-equilibrium state.

higher uptake rate of NH_4 by the small phytoplankton near the surface, and the light may become a limiting factor below 50 m.

The modeled biomass concentrations of small phytoplankton and diatoms, in nitrogen units, are showed in Fig. 5. The modeled small phytoplankton are more abundant than diatoms, which has been suggested from the observations by Bidigare and Ondrusek (1996). The modeled vertical averaged small phytoplankton is 0.131 mmol m^{-3}, and for diatoms, the value is 0.025 mmol m^{-3}. The percentage of diatoms in the total modeled phytoplankton biomass is 16%; the observations indicate that the ratio of diatoms to the total phytoplankton biomass ranges from 5% to 20% (Table 2 in Bidigare and Ondrusek, 1996). The modeled vertical structure of phytoplankton biomass agrees with the observed vertical structure of particulate nitrogen of Chavez et al. (1996) (their Fig. 13), and they do not show the subsurface maximum values. On the other hand, the in situ chlorophyll-*a* measurements showed a chlorophyll maximum at 60 m (Fig. 10 in Bidigare and Ondrusek, 1996). The disagreement of the observed vertical structures between the particulate nitrogen and chlorophyll-*a* implies that the subsurface chlorophyll maximum in the equatorial Pacific is primarily due to increase chlorophyll per cell, in response to decreases in irradiance. Chavez et al. (1996) supported this argument by documenting phytoplankton carbon to chlorophyll ratio decreasing with depth. Eppley et al. (1992) reported that the depth distribution of particulate organic carbon (POC) was uniform over the euphotic zone throughout the region of elevated

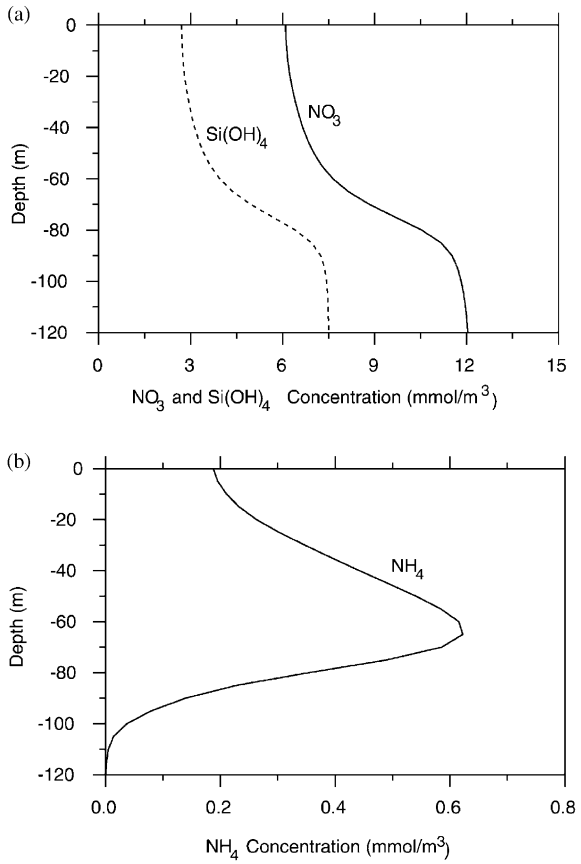

Fig. 4. Modeled vertical profiles at the equilibrium state (day 1000): (a) NO_3 and $Si(OH)_4$ concentration (mmol m^{-3}); (b) NH_4 concentration (mmol m^{-3}). The modeled NH_4 shows a subsurface maximum at 60–70 m as the observations suggested (Murray et al., 1995).

nitrate and lacked pronounced subsurface maxima in the eastern equatorial Pacific, whereas the chlorophyll had the maximum at about 50 m with a twofold increase from the surface

The NOAA/OACES (Ocean Atmosphere Carbon Exchange Study conducted by NOAA) cruises made four north–south transects across the equator in the Pacific Ocean both in the spring and in the fall of 1992. The spring of 1992 coincides with the El Niño event, and the normal upwelling condition returned in the fall of 1992. At this early stage of model development, all simulations are carried out for the non-El Niño condition. Hence, comparison of model simulation results will only be made with the NOAA/OACES fall observations. Samples taken from stations within the Wyrtki Box (i.e. 5°S–5°N and 90°W–180°) are sorted out for this comparison. Shown in Fig. 6 are all the TCO_2 measurements made within the Wyrtki Box, mainly along 110°W, 125°W, and 140°W. The model simulation is consistent with the general trend of TCO_2 depth profiles. At depths below 75 m, the model produces higher TCO_2 than the averaged trend of the observed data. Because of spatial variations, we need to expand the modeling efforts to a full three-dimensional structure to simulate these natural variations, and this effort is currently underway.

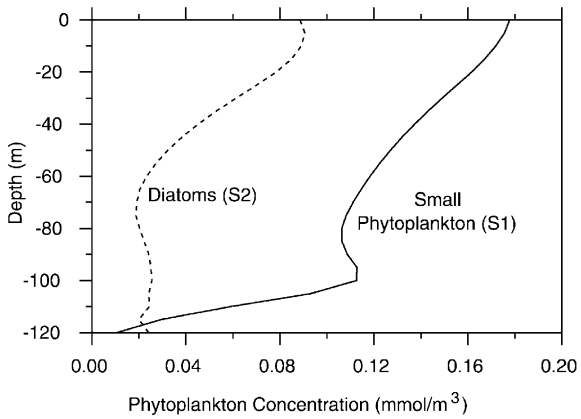

Fig. 5. Modeled vertical profiles of small phytoplankton and diatoms at the equilibrium state (day 1000) (mmol m^{-3}). The modeled small phytoplankton are more abundant than diatoms through the entire water column; the ratio of small phytoplankton to diatoms is about 2–1.

3.2. The balance of the modeled rates of nitrogen and silicon flux

The nitrogen and silicon flow through the one-dimensional model is presented for steady state with the modeled rates and integrated (0–120 m) concentration for each component (Fig. 7). The dominant pathway for nitrogen is through grazing of small phytoplankton by the microzooplankton, releasing of NH_4 by the microzooplankton, to support the N-requirement of the small phytoplankton. The predation of microzooplankton by the mesozooplankton is also relatively large (3.39 mmol m^{-2} day^{-1}), but most of the consumed nitrogen is released into the NH_4 pool by the mesozooplankton (3.29 mmol m^{-2} day^{-1}). The nitrate uptake by small phytoplankton is less than NH_4, 1.11 vs. 6.02 mmol m^{-2} day^{-1}. So, the modeled *f*-ratio for small phytoplankton is 0.16 [1.11/(1.11 + 6.02)]. We have assumed that nitrogen to silicon ratio for diatoms is 1–1 (Brzezinski, 1985). Nitrate and NH_4 are the two sources for nitrogen requirement by the diatoms. The diatoms take up NH_4 according to Michaelis–Menten equation (Eq. (17)), and the rest of the nitrogen to make up nitrogen to silicon ratio equals 1 (Eq. (3)) comes from nitrate. The total nitrate uptake by both small phytoplankton and diatoms is 1.96 (1.11 + 0.85) mmol m^{-2} day^{-1}, which equals to the physical supply of nitrate by the upwelling and vertical diffusion, 1.98 mmol m^{-2} day^{-1}. The physical supply of silicate is less than the nitrate supply, 1.64 mmol m^{-2} day^{-1}, because of the lower source silicate concentration of 7.5 mmol m^{-3} at 120 m, compared to source nitrate concentration of 12.0 mmol m^{-3}. The diatoms take up all the silicate supplied to the euphotic zone by the physics, along with the same amount of nitrogen. The majority of newly grown diatoms are grazed by the mesozooplankton; only small portion of diatoms, $<10\%$, sinks directly. Our approach to the production of detrital nitrogen and silicon is that the mesozooplankton retain N but not silicon after grazing. The amount of exported silicon as detritus (1.52 mmol m^{-2} day^{-1}) plus the amount due to the diatoms sinking (0.08 mmol m^{-2} day^{-1}) are balanced by the physical supply of silicate (1.64 mmol m^{-2} day^{-1}). In contrast, there are three components that contribute to nitrogen export: the detrital nitrogen; the amount due to diatom sinking and the loss term by transfer of N by mesozooplankton to higher trophic levels. The sum of these three terms balances the physical supply of nitrate.

The modeled vertically integrated (0–120 m) daily rates are compared with the US JGOFS EqPac measurements (fall cruises only), in Table 2 along with results from an earlier simple model calculation for 0, 140°W (Dugdale and Wilkerson, 1998). Overall, the modeled rates agree with the JGOFS EqPac measurements, although some of the modeled rates tend to be slightly lower. The model is designed to cover

Table 2
Modeled rates compared with observations

	This modeling study, 5°N–5°S, 90°W–180°	JGOFS EqPac 5°N–5°S, 140°W, fall cruise	JGOFS EqPac 0°, 140°W, fall cruise	Dugdale and Wilkerson (1998) 0°, 140°W
Physical supply of NO_3 (mmol $N\,m^{-2}\,d^{-1}$)	1.98	2.6 (Spring, 92) Ku et al. (1995)	3.4 (Spring, 92) Ku et al. (1995)	3.97
Physical supply of $Si(OH)_4$ (mmol $Si\,m^{-2}\,d^{-1}$)	1.64	2.1 (Spring, 92) Ku et al. (1995)	2.6 (Spring, 92) Ku et al. (1995)	2.36
Primary production (mmol $C\,m^{-2}\,d^{-1}$)	64	91 Barber et al. (1996)	129 Barber et al. (1996)	76
Phytoplankton specific growth rate (d^{-1})	0.46	0.78 (2N–2S) Landry et al. (1995)	0.57 Landry et al. (1995)	0.67
Uptake of NH_4 (mmol $N\,m^{-2}\,d^{-1}$)	6.81	11.82 McCarthy et al. (1996)	15.89 McCarthy et al. (1996)	9.20
Uptake of $Si(OH)_4$ (mmol $m^{-2}\,d^{-1}$)	1.64		1.32 Dam et al. (1995)	2.36
Uptake of NO_3 (mmol $N\,m^{-2}\,d^{-1}$)	1.96	1.97 McCarthy et al. (1996)	2.62 McCarthy et al. (1996)	2.36
Mesozooplankton predation on microzooplankton (mmol $N\,m^{-2}\,d^{-1}$)	3.39	3.03 (= 40% × 7.58) Dam et al. (1995), Landry et al. (1995)	4.3 (= 40% × 10.75) Dam et al. (1995) Landry et al. (1995)	0.69
Mesozooplankton grazing on diatoms (mmol $N\,m^{-2}\,d^{-1}$)	1.64	0.63 Zhang et al. (1995)	0.74 Dam et al. (1995)	2.29
Microzooplankton grazing on small phytoplankton (mmol $N\,m^{-2}\,d^{-1}$)	7.07	7.58 Landry et al. (1995)	10.75 Landry et al. (1995)	8.28
Specific grazing rate on small phytoplankton (d^{-1})	0.45	0.42 (2N–2S) Landry et al. (1995)	0.38 Landry et al. (1995)	
NH_4 supplied from microzooplankton (mmol $N\,m^{-2}\,d^{-1}$)	3.56	4.55 (= 7.58–3.03)	6.45 (= 10.75–4.3)	8.28
NH_4 supplied from mesozooplankton (mmol $N\,m^{-2}\,d^{-1}$)	3.29	0.79 Zhang et al. (1995)	0.52 Zhang et al. (1995)	0.92
Sinking rate of diatoms (mmol $m^{-2}\,d^{-1}$)	0.08			0.034
Faecal pellet production rate (mmol $N\,m^{-2}\,d^{-1}$)	1.48(Si) + 0.60(N) = 2.08	1.07 Roman and Gauzens (1997)	0.96 Roman and Gauzens (1997)	2.29(Si) + 0.69(N) = 2.96
Loss rate to higher trophic level (mmol $N\,m^{-2}\,d^{-1}$)	0.77			
Export production of DSi and DN (mmol $m^{-2}\,d^{-1}$)	1.52(Si) + 0.88(N) = 2.40	1.56 Murray et al. (1996)	1.52 Murray et al. (1996)	2.36(Si) + 0.76(N) = 3.12

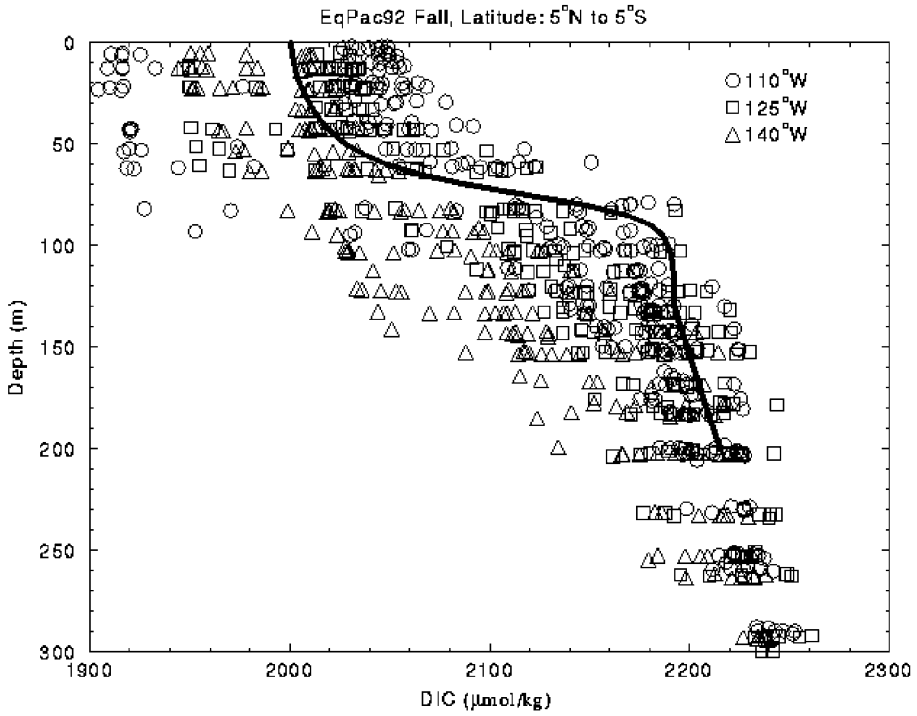

Fig. 6. Comparison between the modeled TCO_2 at the equilibrium state (day 1000) and the observations. The NOAA/OACES (Ocean Atmosphere Carbon Exchange Study conducted by NOAA) cruises made four north–south transects across the equator in the Pacific Ocean in 1992. Samples during the fall cruises taken from stations within the Wyrtki Box (i.e. 5°S–5°N and 90°W–180°) are sorted out for this comparison, mainly along 110°W, 125°W, and 140°W. The model simulation is consistent with the general trend of TCO_2 depth profiles.

the entire Wyrtki Box under the annual mean conditions, whereas the shipboard measurements were collected only along 140°W during the fall of 1992. The averaged phytoplankton specific growth rate is $0.45\,day^{-1}$ in the model, compared to $0.53–0.78\,day^{-1}$ during JGOFS, (Landry et al., 1995). Removal of small phytoplankton growth by microzooplankton grazing each day in the model is close to 100%, which is comparable with the observations of 53–83% by Landry et al. (1995) and 133% by Verity et al. (1996). The modeled mesozooplankton grazing rate on diatoms is $1.48\,mmol\,m^{-2}\,day^{-1}$, agrees with Dam's estimate (Dam et al., 1995) of $0.73\,mmol\,m^{-2}\,day^{-1}$. Dam et al. (1995) reported that mesozooplankton only removed 1–9% of the daily growth of chlorophyll, which could be all due to diatoms (Bidigare and Ondrusek, 1996). The modeled predation rate by mesozooplankton is in good agreement with the estimates by Dam et al. (1995) and Zhang et al. (1995). Both authors suggested that mesozooplankton must ingest a large portion microzooplankton and detritus to satisfy their daily carbon requirements. The modeled NH_4 supplied from mesozooplankton excretion is $3.29\,mmol\,m^{-2}\,day^{-1}$, which is higher than the observations $0.52–0.79\,mmol\,m^{-2}\,day^{-1}$ (Zhang et al., 1995). On the other hand, total NH_4 supplied both from microzooplankton and mesozooplankton ($6.85\,mmol\,m^{-2}\,day^{-1}$) agrees well with the observations 5.34–$6.97\,mmol\,m^{-2}\,day^{-1}$ (Zhang et al., 1995). The export production in the model is defined as the sum of sinking detrital nitrogen and silicon and sinking diatoms, which is $2.40\,mmol\,N\,m^{-2}\,day^{-1}$. The modeled export production compares well with the higher estimates obtained using sediment traps 1.52–1.56 mmol $N\,m^{-2}\,day^{-1}$ (Murray et al., 1996), but about a factor of 3–5 higher than the lower estimates 0.31–$1.06\,mmol\,N\,m^{-2}\,day^{-1}$ by Busseler et al. (1995) and Bacon et al. (1996). Murray et al. (1996) discussed some of the difference in the export production estimates by different authors, the key factor could be the

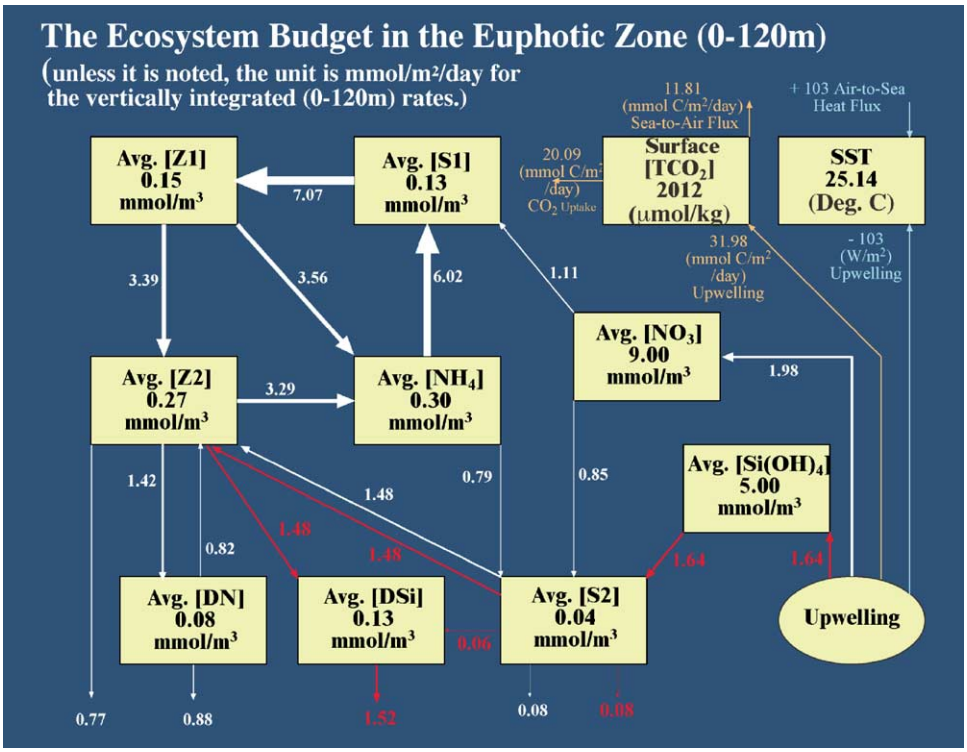

Fig. 7. The model budget for nitrogen, silicate, TCO_2, and heat at the equilibrium state (day 1000). The ecosystem variables are averaged in the euphotic zone (0–120 m), the unit is mmol m^{-3}. The TCO_2 and SST are used instead of vertically averaged values. All the rates are vertically integrated from 0 to 120 m, the unit is mmol m^{-2} day^{-1}. The width of each line is proportional to the value of the rate. The white lines indicate the flow of nitrogen, the red lines are for the silicate, dark yellow lines are for the carbon flow, and green lines show the heat balance.

organic carbon to ^{234}Th ratio which is used to convert the activities of ^{234}Th into the export of POC in carbon unit. In our modeled export production, silicon to nitrogen ratio is about 2–1, 1.52 vs. 0.88 mmol m^{-2} day^{-1}. Dunne et al. (1999) suggested that silicon fluxes appear tightly coupled to nitrogen fluxes during EqPac survey II cruise, but not during other three cruises (Fig. 4 in Dunne et al., 1999). Some of mechanisms for nitrogen and silicon decoupling were discussed by Dunne et al. (1999), such as particulate organic nitrogen remineralization and silica dissolution. Considering simple physical forcing (upwelling and vertical diffusivity) used in this model and under the steady-state condition, the modeled rates compare with the observations reasonable well.

3.3. Diatom growth regulated by Si and light

The uptake of $Si(OH)_4$ by diatoms is clearly regulated by light and silicate concentration, Eq. (16). The depth profile of $Si(OH)_4$ uptake depends upon the how light is treated in the model as well as the vertical supply of $Si(OH)_4$ by the upwelling and vertical mixing. For example, if the upwelling and vertical mixing supply too much $Si(OH)_4$ into the upper euphotic zone, which could result in $Si(OH)_4$ concentration $\gg K_{Si(OH)_4}$, then $Si(OH)_4$ uptake would increase and the diatom population would increase until a balance between uptake and supply was re-established. As depth increases, a point is reached below which the rate of uptake is limited by light rather than by $Si(OH)_4$. The upwelling rate and vertical mixing coefficient in the

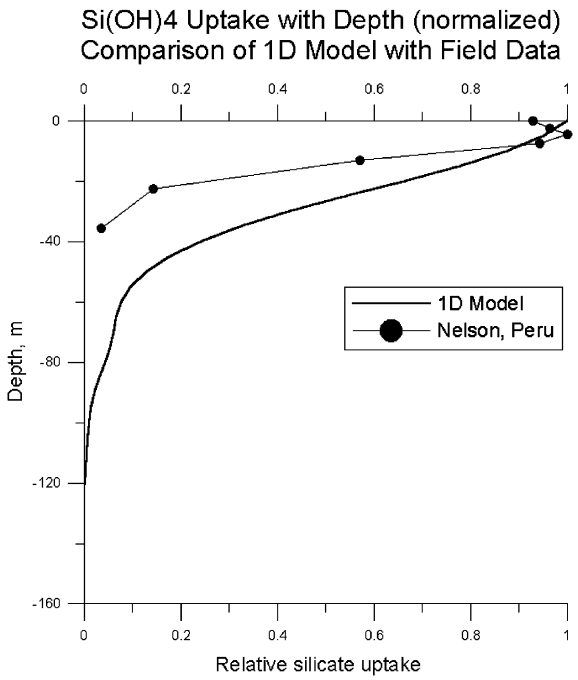

Fig. 8. Comparison between the modeled (daily averaged) and observed normalized (to the maximum values) silicate uptake rate, ρSi(OH)4 (NPS2 in the Eq. (16)) plotted against depth. The measurements by Nelson et al. (1981, their Fig. 3) for the averaged $Si(OH)_4$ uptake under the weak wind conditions off Peru coast was used (dash-dot line). The general shape of our modeled vertical $Si(OH)_4$ uptake is in agreement with the measurements off Peru coast, which indicates the model captured the essential processes that determine $Si(OH)_4$ uptake, i.e. the light treatment and supply of $Si(OH)_4$ by the upwelling and mixing.

model have been adjusted and validated by the heat balance, Fig. 3a. Examination of the vertical profile of $Si(OH)_4$ uptake and comparison with the limited direct $Si(OH)_4$ uptake measurements provides additional validation for the model. Direct measurements of $Si(OH)_4$ uptake are rarely conducted in the open ocean. Therefore, we compare vertical profile of $Si(OH)_4$ uptake from a coastal station with our one-dimensional modeled results. Fig. 8 shows the vertical profile of the modeled $\rho Si(OH)_4$ (NPS2 in the Eq. 16) normalized to the maximum value, and the measurements (also normalized to the maximum) by Nelson et al. (1981, their Fig. 3) for the averaged $Si(OH)_4$ uptake under the weak wind conditions off Peru coast. The general shape of our modeled vertical $Si(OH)_4$ uptake is in agreement with the measurements off Peru coast, which indicates the model captured the essential processes that determine $Si(OH)_4$ uptake, i.e. the light treatment and supply of $Si(OH)_4$ by the upwelling and mixing. In the model, small amount of $Si(OH)_4$ uptake occurs below the 1% of surface light level. The measurements by Leynaert et al. (2001) suggest that uptake $Si(OH)_4$ during night were very small (Fig. 4 in Leynaert et al., 2001). Dugdale et al. (2002) present more detailed comparisons between our modeled results with the measurements by Leynaert et al. (2001).

3.4. The sea-to-air CO_2 flux

In the model, the biological removal of TCO_2 in the euphotic zone is linked, through Redfield C/N ratio, with the uptake of NO_3 and $Si(OH)_4$ by both small phytoplankton and diatoms. Unlike nitrogen and silicon, there is a surface sea-to-air flux of CO_2 for the TCO_2. The upwelling brings up high TCO_2 water to the surface, the pCO_2 in the surface water is higher that the pCO_2 in the air, therefore, there is a net flux. To

Table 3
Comparison of model estimate of CO_2 evasion flux with those based on field observations in the equatorial Pacific during non-El Niño conditions

Region of interests	Year of survey	Annual CO_2 flux ($mol\,m^{-2}\,yr^{-1}$)	References
5°S–5°N, 100°W–170°E	1979–80	4.5	Keeling and Revelle (1985)
10°S–10°N, 80°W–150°E	1979–80	2.2	Smethie et al. (1985)
10°S–10°N, 80°W–130°E	1979–80	1.9	Takahashi et al. (1986)
10°S–10°N, 80°W–135°E	1984	1.4	Feely et al. (1987)
10°S–10°N, 80°W–120°E	1984	1.7	Volk (1989)
10°S–10°N, 170°W–180°W	1989	1.0	Wong et al. (1993)
5.5°S–5.5°N, 80.5W–134.5E	1989	3.8	Inoue and Sugimura (1992)
10°S–10°N, 95°W–140°W	1992	1.4	Feely et al. (1997)
10°S–10°N, 95°W–140°W	1994	2.5	Feely et al. (1997)
5°S–5°N, 90°W–180°W	Modeled annual mean	4.3	This modeling study

simulate the TCO_2 flux at the air–sea interface, the atmospheric pCO_2 is assumed to be constant at 357 ppm, which corresponds to 1992 conditions (Feely et al., 1987).

The average model CO_2 evasion flux across the sea–air interface is estimated to be about $4.3\,mol\,m^{-2}\,yr^{-1}$. As summarized in Table 3, there are a few estimates of annual CO_2 flux during the non-El Niño conditions in the equatorial Pacific. They range from 1.0 to $4.5\,mol\,m^{-2}\,yr^{-1}$. This model estimate is consistent with the range of the observed results. Based on these comparisons, we conclude that the basic structure of the model is sufficiently sound to produce the key variable values that are consistent with the first order features observed in this region. In order to simulate the air–sea flux of CO_2 with detailed spatial distribution and temporal variation, a complete three-dimensional simulation of the carbon cycle is needed.

3.5. Sensitivity analysis

With one set of the parameters used (Table 1), the model reproduced the mean state in the "Wyrtki Box" (Figs. 4–7, Tables 2 and 3). The modeled mean state is defined as the "standard" run, which provides a base for a series of parameter sensitivity analyses. There are 25 biological parameters in the model that can be varied, together with the upwelling velocity, vertical diffusivity, and nutrient concentrations below the euphotic zone. In this paper, we present several examples on how the sensitivity analyses were conducted throughout our model development. The paper by Dugdale et al. (2002) discusses the model responses to the changes of silicate concentration below the euphotic zone.

We have developed a method that allows us to vary one or more parameters independently throughout a wide range for each parameter. By varying one parameter at a time, we run the model until it reaches the steady state, and analyze the model results at day 1000. To analyze the model sensitivity, the modeled properties (concentrations and rates) can be plotted against that particular varying parameter. This technique also allows us to test different combinations of two parameters. In this case, following the isolines for different state variables (nitrate, silicate, etc.) and rates (primary production, grazing rates, etc.) would provide some guidelines on how to search for a "right" combination of two parameters. Similar experiments can be done by varying three parameters, then the iso-surfaces of different state variables and rates can be examined. In theory, the model sensitivity can be examined by varying all the parameters but analyzing and presenting the results from such experiments are nearly impossible. Over the course of our model development, we have conducted more than 200,000 model runs to test the model sensitivity to different parameters. Of course, all the state variables and related rates for various parameter values can be

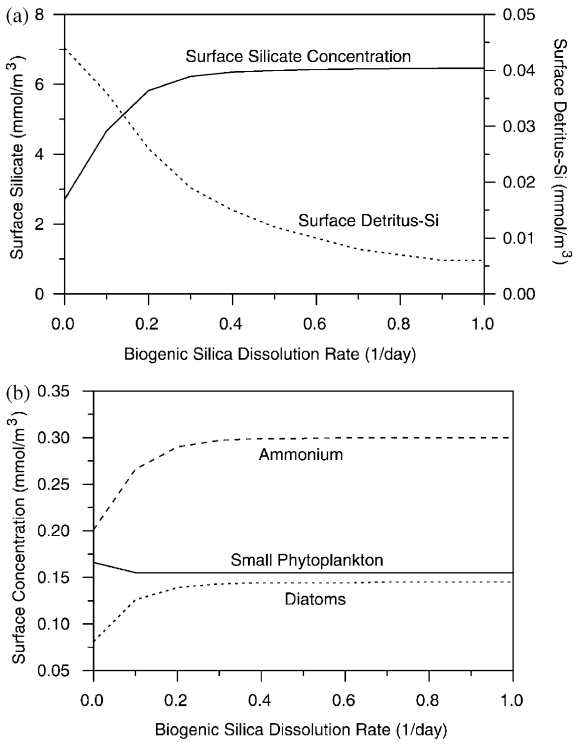

Fig. 9. Surface response of the one-dimensional model to changes in the parameter γ_4 (the biogenic silica dissolution rate): (a) $Si(OH)_4$ and DSi concentration (mmol m^{-3}); (b) small phytoplankton, diatoms, and NH_4 concentration (mmol m^{-3}).

shown, but that will lead to too many figures considering a number of varying parameters. In this paper, we focus our analyses on the surface nutrient and phytoplankton concentrations at the end of 1000-day model simulations. Due to the limited space and scope of this paper, we can only present a few model sensitivity runs and discuss the results.

First, the model sensitivity to biogenic silica dissolution rate, parameter γ_4 in the Eqs. (4) and (11), was tested with the model by varying γ_4 from 0.0 to 1.0 day^{-1}. Fig. 9 shows the modeled surface silicate concentration, detritus, ammonium, and diatom concentration, which are all strongly sensitive with γ_4 in the range of 0–0.2 day^{-1}. The modeled results at low dissolution rates agree well with the JGOFS data, such as the mean surface silicate concentrations for all four JGOFS EqPac cruises which ranged from 2.2 to 3.8 mmol m^{-3} (Dugdale et al., 2002, Table 2). In order to match the modeled surface silicate concentration, the biogenic silica dissolution rate has to be in a range of about 0–0.05 day^{-1} (Fig. 9a). The concentrations of small phytoplankton and diatoms found by Chavez et al. (1991) was 0.2 and 0.088 mmol N m^{-3}, the ratio of small phytoplankton to diatoms is about 2.3. With the dissolution rate set to zero in the model, the both concentrations of small phytoplankton and diatoms (Fig. 9b), as well as small phytoplankton to diatoms ratio (2.1 in the model), agree well with the Chavez et al. (1991) data. The modeled results diverge strongly from data at higher dissolution rates. The modeled surface ammonium concentration at dissolution rate of zero is at the top of the observed concentrations during the JGOFS cruises, which range from 0.02 to 0.2 mmol m^{-3}.

Using a global average silica dissolution:production ratio of 0.5 from Nelson et al. (1995), we can estimate indirectly biogenic silica dissolution rate by combining the modeled diatom production (or uptake rate of silicate) and mean concentration of detrital silica (biogenic silica). The diatom production in the

model is 1.64 mmol m^{-2} day^{-1} in the upper 120 m that balances the supply of silicate (Fig. 7), Which is equivalent to an average silica production rate of $1.64/120 = 0.01367$ mmol m^{-3} day^{-1}. So, the silica dissolution rate would be 0.00683 mmol m^{-3} day^{-1} (0.5×0.01367) in the model if the silica dissolution:-production ratio of 0.5 is applied. Given the low detrital silica concentration in the euphotic zone, 0.13 mmol m^{-3} (Fig. 7), then expected specific dissolution rate would be 0.05 day^{-1} (0.00683/0.13). According to Fig. 9, the dissolution rate of 0.05 day^{-1} will result in a relatively small change in surface silicate concentrations, ammonium concentrations, detrital silica concentrations, etc. Even with a relatively high dissolution:production ratio for the equatorial Pacific, such as 0.5, it would not change the model results significantly.

The biogenic silica dissolution rates have not been measured directly in the equatorial Pacific. Low dissolution rates, <0.1 day^{-1}, have been measured in the Peru upwelling area by Nelson et al. (1981) who felt the rate of dissolution to be insignificant relative to silicate uptake. Brzezinski et al. (1997) reported the Si dissolution to production ratio to be in the range of 0.05–0.15 in the Big Sur area off California. Indirectly measured high rates of dissolution, i.e. >0.5, have been published for some oligotrophic areas such as Sargasso Sea and in the upwelling area off northwest Africa. In the absence of direct measurements of biogenic silica dissolution rate in the equatorial Pacific, and because the modeled results are in good agreement with the field data, we feel that the dissolution rate of zero in the current one-dimensional model to be appropriate. The biogenic silica dissolution rate for the equatorial Pacific needs to be investigated further both in modeling as well as with observations.

Second, we change the parameter α (the initial slope of the photosynthetic rate over irradiance at low irradiance) for diatom silicate uptake only, α is not changed in the small phytoplankton uptake calculation for this sensitivity analysis. When α is changed from 0.005 to 0.05 $(W/m^2)^{-1}$ day^{-1}, with an incremental of 0.005 $(W/m^2)^{-1}$ day^{-1}, the diatom population increases and the small phytoplankton decreases initially. After α reaches the value of 0.02 $(W/m^2)^{-1}$ day^{-1}, both phytoplankton populations level off, Fig. 10b. The changes in phytoplankton populations result in the initial decrease of silicate and increase of nitrate, Fig. 10a. The initial increase of diatoms corresponding to the increase in α likely represents the decrease of iron limitation for diatom growth. Once α reaches 0.02 $(W/m^2)^{-1}$ day^{-1}, the surface silicate concentration is about 3.0 mmol m^{-3} that is near the half-saturation concentration ($K_{Si(OH)_4}$) for silicate uptake by diatoms. The decrease of small phytoplankton is due to increase of ammonium concentration that enhances the effects of inhibition of nitrate uptake by small phytoplankton. Under the steady-state conditions, the silicate becomes the major limiting factor after α exceeds 0.02 $(W/m^2)^{-1}$ day^{-1}. A value of 0.025 $(W/m^2)^{-1}$ day^{-1} for α gave the modeled surface nutrient concentrations, diatom concentration, and its percentage in the total phytoplankton ($<18\%$) closest to those observed.

The rate of silicate uptake by diatoms is also affected by the value of $K_{Si(OH)_4}$, see Eq. (16). The $K_{Si(OH)_4}$ was changed from 0.5 to 5.0 mmol m^{-3}, with an incremental of 0.5 mmol m^{-3} for each experiment. By increasing the $K_{Si(OH)_4}$, the modeled surface silicate concentration increases, and the diatom population decreases (Fig. 11). The surface nitrate concentration is relatively insensitive to the change of $K_{Si(OH)_4}$. This suggests that for a given supply of silicate by the physical processes, the surface silicate concentration is very sensitive to the half-saturation concentration of silicate uptake. Under the steady-state conditions, the modeled surface silicate concentration is close to the value of the half-saturation concentration of silicate uptake (Fig. 11a). The observed surface silicate concentration is about 3.0 mmol m^{-3} (Dugdale and Wilkerson, 1998), a value of 3.0 mmol m^{-3} for the $K_{Si(OH)_4}$ was selected for the "standard" model run.

The model separates nitrate and ammonium into two nitrogen pools, and it allows us to address the new and regenerated production for small phytoplankton and diatoms (Dugdale and Goering, 1967). As ammonium is preferentially used by phytoplankton (Dortch, 1990), the effect of inhibition of nitrate uptake by ammonium (Wheeler and Kokkinakis, 1990) has to be included in the model. The ammonium inhibition effect was calculated as an exponential function of the ammonium concentration (see Eq. (12)), which is similar to the treatments by several previous studies (Wroblewski, 1977; Fasham et al., 1990; Price et al.,

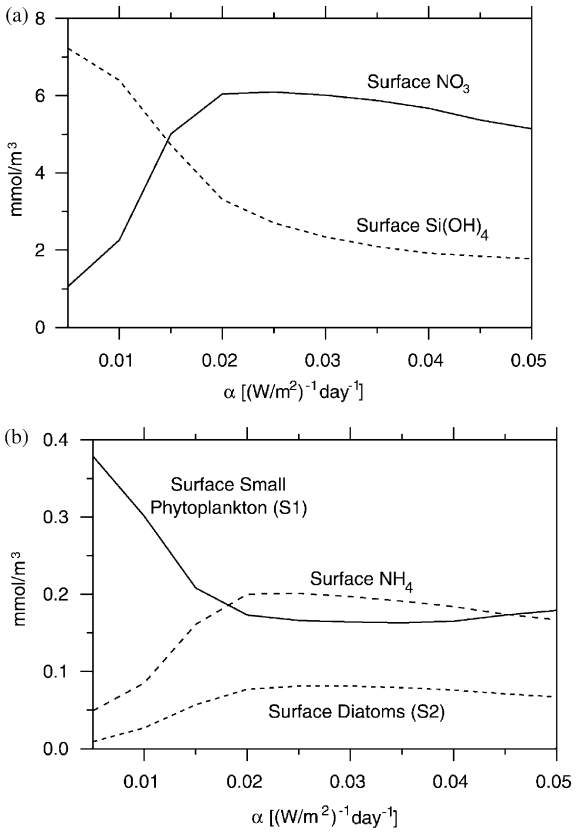

Fig. 10. Surface response of the one-dimensional model to changes in the parameter α (the initial slope of the photosynthetic rate over irradiance at low irradiance) for diatom silicate uptake: (a) NO_3 and $Si(OH)_4$ concentration (mmol m^{-3}); (b) small phytoplankton, diatoms, and NH_4 concentration (mmol m^{-3}).

1994). The degree of ammonium inhibition increases as ψ (the inhibition parameter) is increased. To demonstrate the sensitivity of parameter ψ on ammonium inhibition, we varied ψ between 1.0 and 10.0 (mmol m^{-3})$^{-1}$ with an increments of 1.0 (mmol m^{-3})$^{-1}$. The modeled surface nitrate concentration changed from 0.8 mmol m^{-3} for $\psi = 1.0$ (mmol m^{-3})$^{-1}$ to 7.4 mmol m^{-3} for $\psi = 10.0$ (mmol m^{-3})$^{-1}$, Fig. 12a. The sharp increase of nitrate concentration with increasing ψ values also was found in a model sensitivity study by (Fig. 15d in Fasham, 1995). The modeled surface small phytoplankton decreased sharply between $\psi = 1.0$ and 5.0 (mmol m^{-3})$^{-1}$, and was less sensitive beyond ψ large than 6.0 (mmol m^{-3})$^{-1}$, Fig. 12b. The modeled diatom population increased gradually with increasing ψ values (Fig. 12b). This is because the grazing pressure on diatoms by mesozooplankton decreased with increasing ψ values, the modeled micro- and meso-zooplankton concentrations are shown in Fig. 12c. At low ψ values, the small phytoplankton concentration was high, and resulted in higher grazing by microzooplankton, which benefited mesozooplankton. With increasing ψ values, the mesozooplankton decreased and diatoms increased, and caused surface silicate concentration to decrease (Fig. 12a). Throughout the entire range of ψ values, the microzooplankton biomass stayed relatively unchanged, but grazing rate by the microzooplankton decreased proportionally to the decrease of small phytoplankton (not shown); further it was reflected in decreasing predation rate by the mesozooplankton. Based upon the modeled surface

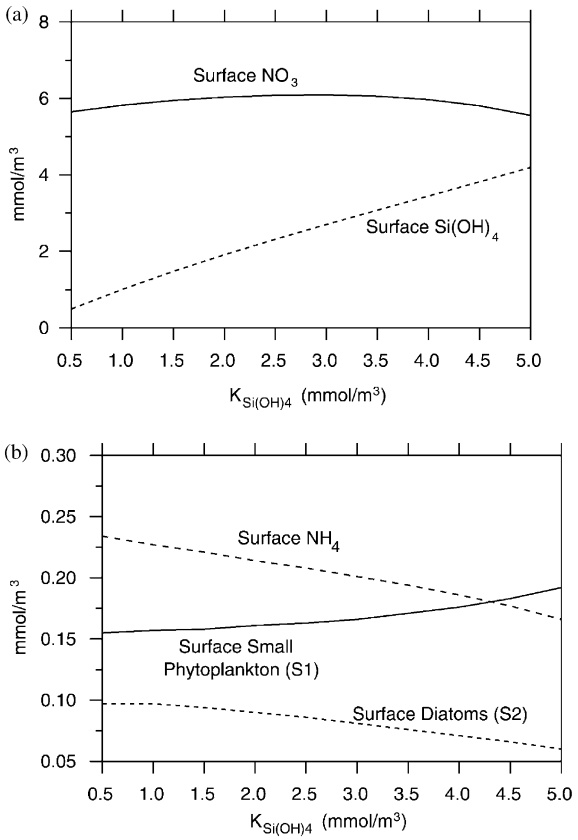

Fig. 11. Surface response of the one-dimensional model to changes in the parameter $K_{Si(OH)_4}$ (the half-saturation concentration for silicate uptake by diatoms): (a) NO_3 and $Si(OH)_4$ concentration (mmol m^{-3}); (b) small phytoplankton, diatoms, and NH_4 concentration (mmol m^{-3}).

concentrations and the observed mean nitrate and silicate concentration in the equatorial region, a ψ value of 5.59 (mmol m^{-3})$^{-1}$ was selected in the "standard" model run. This value is in agreement with the suggestion by Wheeler and Kokkinakis (1990).

The idea that zooplankton grazing contributes to the control of phytoplankton biomass has exited biological oceanographers for more than 20 years. Walsh (1976) was the first to argue that grazing (or overgrazing), not vigorous circulation or micronutrient deficiency, was the process maintaining equatorial phytoplankton biomass at anomalously low levels. Frost (1987, 1991) analyzed both model results and field data at Ocean Station P (50°N, 145°W) and summarized the role of grazing in the nutrient-rich areas of the open ocean. With this ecosystem model, the role of zooplankton grazing in the equatorial Pacific can be tested by conducting a series of sensitivity studies.

The effect of mesozooplankton grazing was studied by varying the parameters $G2_{max}$, the mesozooplankton maximum grazing rates. The $G2_{max}$ was changed between 0.4 and 0.6 day^{-1}, with an incremental of 0.025 day^{-1}. By increasing the $G2_{max}$, the modeled surface silicate concentration increases, and diatom population decreased (Fig. 13a and b). The mesozooplankton increased sharply with increasing $G2_{max}$, which drove the diatoms toward lower concentration (Fig. 13c). The surface nitrate decreased with increasing the $G2_{max}$, because of the increase in small phytoplankton biomass. The ammonium concentration decreased sharply beyond $G2_{max} = 0.525$ day^{-1}, which relaxed the effects of ammonium

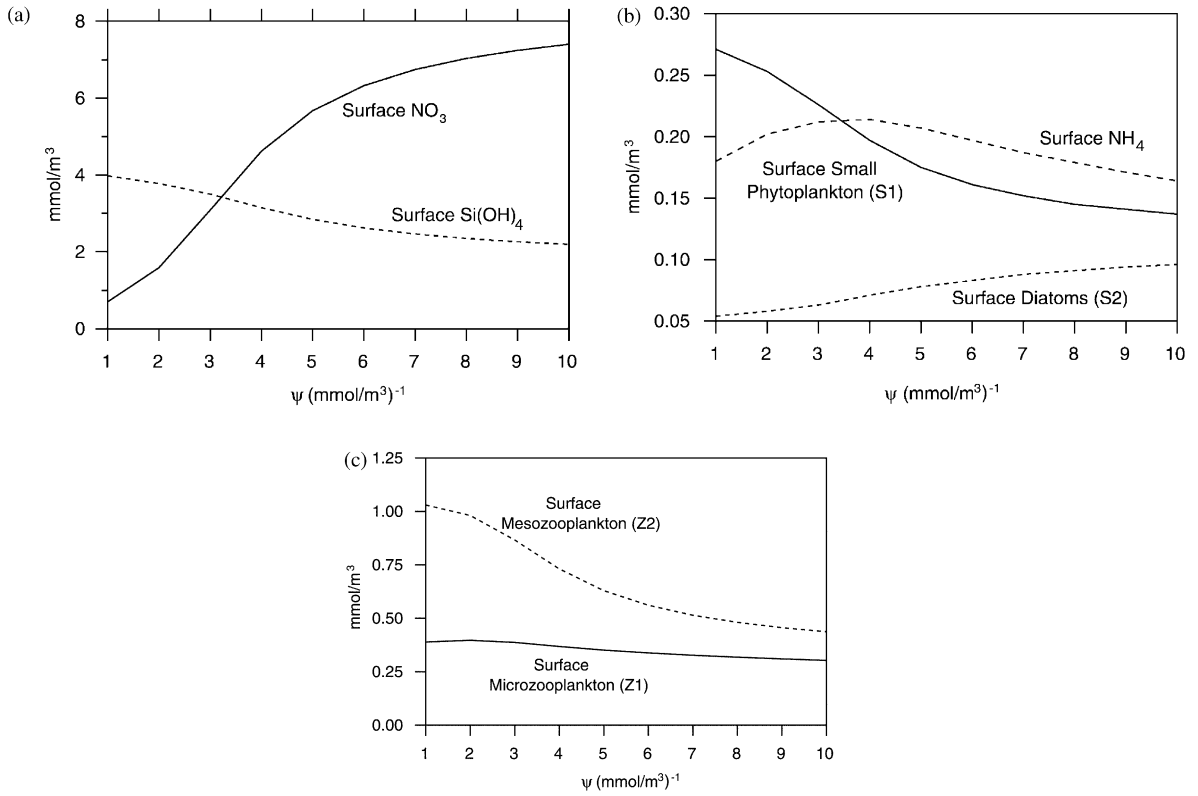

Fig. 12. Surface response of the one-dimensional model to changes in the parameter ψ (the ammonium inhibition parameter): (a) NO_3 and $Si(OH)_4$ concentration, concentration (mmol m^{-3}); (b) small phytoplankton, diatoms, and NH_4 concentration (mmol m^{-3}); (c) micro- and meso-zooplankton concentration (mmol m^{-3}).

inhibition and resulted in an increase in growth of small phytoplankton. The microzooplankton concentration was relatively unchanged throughout most $G2_{max}$ of the runs with different $G2_{max}$ values, except at the end, it decreased slightly. This also would enhanced the small phytoplankton growth. Based upon the observed values of nutrients and phytoplankton concentrations, a value of 0.53 day^{-1} for the $G2_{max}$ was selected for the "standard" model run.

Chai et al. (2000) has documented the importance of the microzooplankton grazing in a simplified ecosystem model for the equatorial Pacific. Similar to the test of mesozooplankton grazing, the effect of microzooplankton grazing can be studied by varying the parameter $G1_{max}$, the microzooplankton maximum grazing rates. But unlike previous sensitivity tests, we varied both parameters $G2_{max}$ and $G1_{max}$ in order to investigate the effects of both micro- and meso-zooplankton grazing. The $G2_{max}$ was changed between 0.4 and 0.6 day^{-1}, with increments of 0.025 day^{-1}, the $G1_{max}$ was changed between 1.0 and 2.0 day^{-1}, with increments of 0.1 day^{-1}. There were a total of 99 model runs in this sensitivity study. The modeled surface nitrate concentration was insensitive to the $G1_{max}$ and $G2_{max}$ in the high values of the $G1_{max}$, Fig. 14a. The surface nitrate concentration increased with increasing $G1_{max}$. The minimum value of $G1_{max}$ has an impact on the surface nitrate concentration when the $G2_{max}$ increased, see 7 mmol m^{-3} isoline of nitrate concentration in Fig. 14a. Also, the isolines of surface nitrate were very close to each other, i.e. a strong gradient, in a certain range of values of $G1_{max}$, which indicates surface nitrate is very sensitive to the changes of $G1_{max}$. For example, if $G2_{max}$ was set to 0.55 day^{-1}, the nitrate would increase from 1 to 7 mmol m^{-3} and silicate would decrease from 4.7 to 2.7 mmol m^{-3} (Fig. 14b) when the $G1_{max}$ changed from

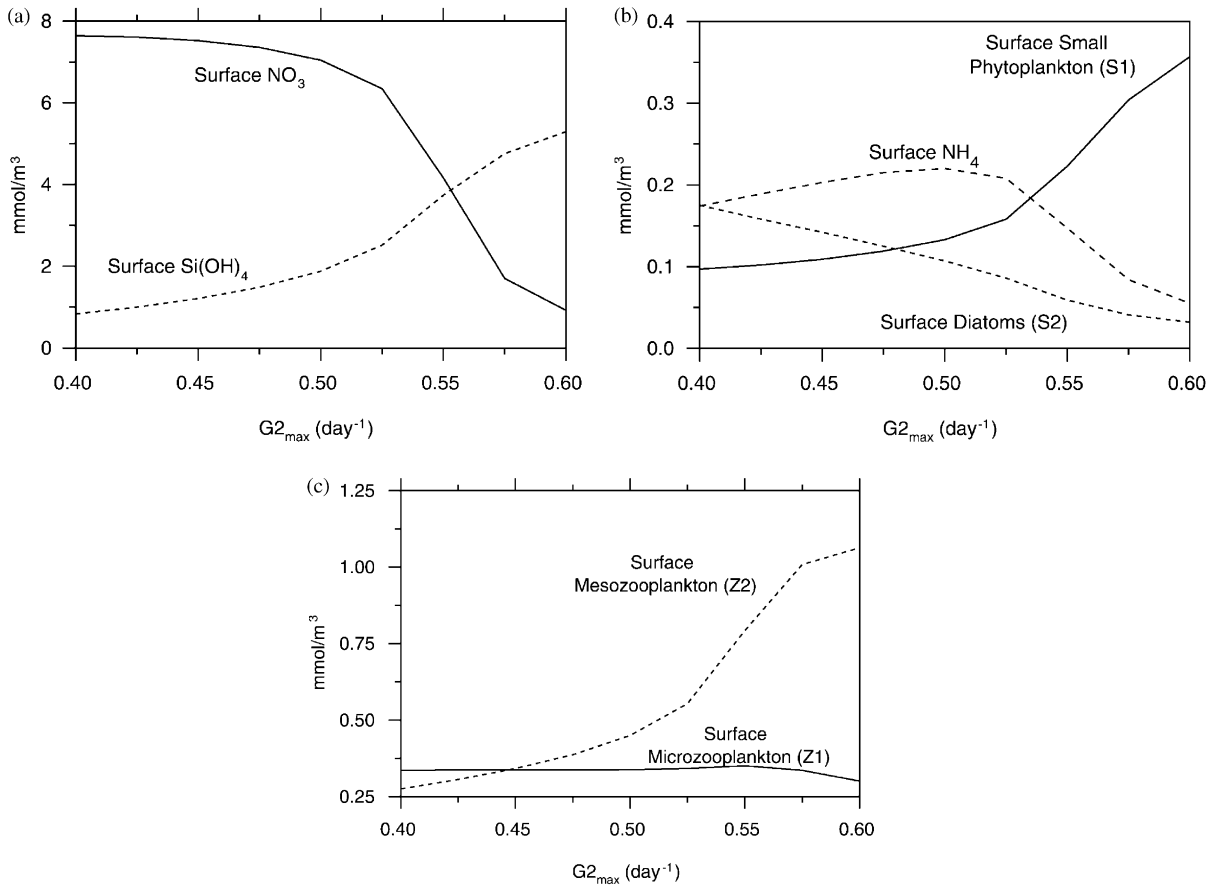

Fig. 13. Surface response of the one-dimensional model to changes in the parameters $G2_{max}$ (the mesozooplankton maximum grazing rates): (a) NO_3 and $Si(OH)_4$ concentration, concentration (mmol m^{-3}); (b) small phytoplankton, diatoms, and NH_4 concentration (mmol m^{-3}); (c) micro- and meso-zooplankton concentration (mmol m^{-3}).

1.2 to 1.5 day^{-1}. Such rapid changes in nitrate concentration are due to the change in small phytoplankton biomass (Fig. 14c). In comparison with nitrate, the modeled surface silicate concentration was less sensitive to the change of $G1_{max}$. It is related to the modeled diatom concentration that is primarily determined by the $G2_{max}$, most isolines of diatom concentration orient vertically (Fig. 14d). In summary, the model is quite sensitive to the zooplankton grazing parameters, a point that already has been made by previous model studies (Frost, 1987, 1991; Fasham, 1995; Chai et al., 2000).

3.6. The role of iron

The importance of iron as a micronutrient regulating phytoplankton productivity has been demonstrated in IronEx-1 and IronEx-2. Both iron-enrichment experiments reported that diatoms were stimulated by iron addition more than other taxonomic forms of phytoplankton (Martin et al., 1994; Coale et al., 1996). During the IronEx-1 experiment, α, the slope of the photosynthetic rate over irradiance at low irradiance, was doubled inside the iron-enriched patch relative to outside the patch where it remained unchanged (Lindley and Barber, 1998). They suggested that iron directly regulate photosynthesis of phytoplankton in surface waters of the HNLC region in the equatorial Pacific Ocean. Hutchins and Bruland (1998) showed

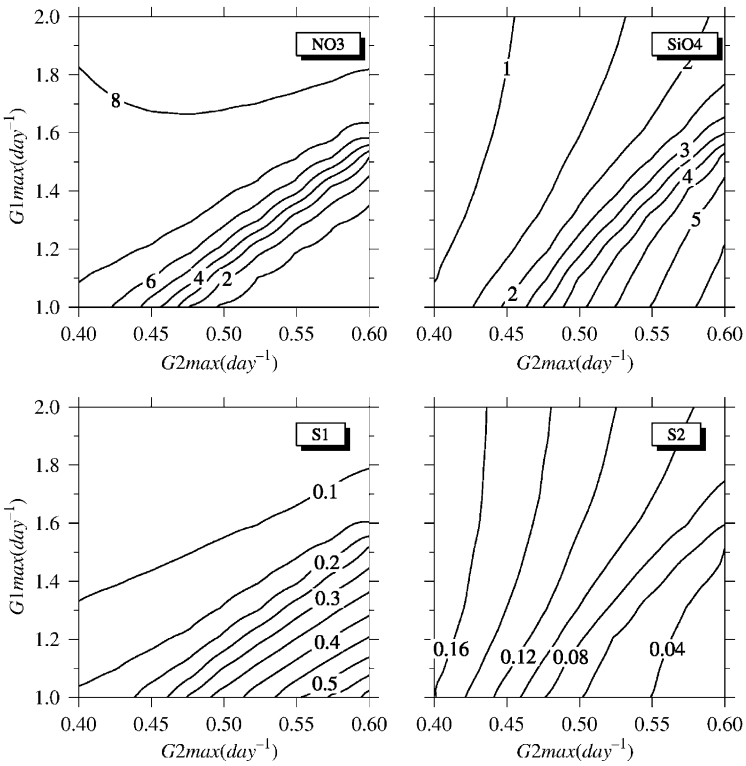

Fig. 14. Surface response of the one-dimensional model to changes in the parameters $G1_{max}$ (the microzooplankton maximum grazing rates) and $G2_{max}$ (the mesozooplankton maximum grazing rates), the unit is mmol m^{-3}.

that iron deficiency could change the Si:N uptake ratio of diatoms, and affect the silicate pump in the HNLC regions. Unfortunately, many previous iron addition experiments did not have silicate uptake measurements, which makes it difficult to understand the relationship between iron and silicate limitation in the HNLC regions.

The current model does not include iron as a limiting nutrient, but rather considers its role implicitly through the parameters that determine the growth rate of diatoms. To model the effects of iron limitation we modify the model in two places as a sensitivity investigation. The first is to change the term α, in the light regulation term of silicate uptake by diatom. The second is to change the term $K_{Si(OH)_4}$; this objective is speculative, but is based on $K_{Si(OH)_4}$ variability in many different oceanic systems and in lab cultures which are iron replete and have low $K_{Si(OH)_4}$. Reported half-saturation values for silicate uptake vary considerably. Nelson and Brzezinski (1990) reported an overall mean value for non-Antarctic diatoms of about 2.3 mmol m^{-3}, while for Antarctic diatoms Nelson and Treguer (1992) reported values >5.0 mmol m^{-3}. Intuitively it seems that the iron effect on silicate uptake is most likely to be involved in initiation of diatom blooms. However, Lindley and Barber (1998) found that in IronEx-2 the diatoms had enhanced, near-maximal quantum yields, so iron photosynthetic effects may be especially important in diatoms. The two iron effects, α and $K_{Si(OH)_4}$, are independent, and in the model simulations they are tested separately and together.

Three model experiments were conducted in order to examine the role of iron. Between days 900 and 930 of the model, the upwelling rate was doubled for all three experiments, which resulted in an injection of iron

into the euphotic zone. After 30 days, the tested parameters and upwelling rate were returned back to the values used in the standard model run. In the Exp-1, α was increased from $0.025\,(W/m^2)^{-1}\,day^{-1}$ (standard model run) to $0.05\,(W/m^2)^{-1}\,day^{-1}$, and $K_{Si(OH)_4}$ was unchanged (i.e., $3.0\,mmol\,m^{-3}$ for the standard). In the Exp-2, α was unchanged, but $K_{Si(OH)_4}$ was decreased from $3.0\,mmol\,m^{-3}$ (standard) to $1.0\,mmol\,m^{-3}$. The Exp-3 was to combine experiments 1 and 2, $\alpha = 0.05\,(W/m^2)^{-1}\,day^{-1}$ $K_{Si(OH)_4} = 1.0\,mmol\,m^{-3}$. All modeled surface concentrations are shown in Fig. 15. The largest change was seen in the Exp-3 followed by the Exp-2. The effects of α and $K_{Si(OH)_4}$ on diatom growth are not linear (see panel D in Fig. 15), which indicates that both parameters have to be altered in order to get a larger diatom bloom. 15 days after the experiments (day 945), biomass of both small phytoplankton and diatoms returned to the values in the standard model experiment, the microzooplankton biomass was slightly higher than the standard value, but the mesozooplankton nearly doubled in biomass during Exp-3 and stayed high. It might take much longer for the model itself to lose all excess mesozooplankton, whereas in nature, the higher trophic levels will consume the mesozooplankton easily and quickly.

To examine the relationships among the components, the modeled surface concentrations during the Exp-3 are shown in Fig. 16. Within the first 5 days, the diatom biomass increased from 0.08 to $2.5\,mmol\,m^{-3}$, more than a factor of 30 increase. But the diatom populations crashed at day 912, 12 days after the experiment started, due to exhaustion of available silicate and increased mesozooplankton. It seems that the mesozooplankton populations responded to the increase of diatoms too quickly in the model, which may be because the current model does not include mesozooplankton reproduction cycle. In nature, the increase in mesozooplankton biomass should lag the increase in diatom populations by 7–10 days (Monger et al., 1997). During the first 10 days in the experiment, the small phytoplankton populations were decreased due to the increase of microzooplankton. Gradually, the mesozooplankton grazed down the microzooplankton, which resulted in a relaxation in grazing pressure on the small phytoplankton by the microzooplankton. The ammonium concentration increased from day 5 to 13, because of the increase in both micro- and meso-zooplankton concentrations. The increased ammonium concentration enhanced growth of small phytoplankton; by day 15 into the experiment, they reached the highest concentration $0.7\,mmol\,m^{-3}$. Compared to the "standard" experiment concentration for small phytoplankton concentration of $0.2\,mmol\,m^{-3}$ this is about a factor of 3 increase during Exp-3. Two days after the small phytoplankton peaked, the maximal biomass of microzooplankton. Such a cycle was repeated a few times, but the amplitude of the oscillation became smaller each time. In response to the change of the microzooplankton populations, the mesozooplankton also oscillated reaching peaks 2 or 3 days after the microzooplankton. 45 days (day 975) after the Exp-3 ended, the mesozooplankton concentration was about $1.0\,mmol\,m^{-3}$, which was higher than the standard experiment ($0.6\,mmol\,m^{-3}$). It resulted in keeping diatom concentration at a lower level, $0.04\,mmol\,m^{-3}$ compared to $0.08\,mmol\,m^{-3}$ in the standard experiment.

There have not been any direct measurements showing availability of iron to affect the parameter $K_{Si(OH)_4}$ used in the diatom uptake calculation, lowering $K_{Si(OH)_4}$ to reflect increase of iron, therefore, is speculative. De La Rocha et al. (2000) have shown that there is no effect of iron on $K_{Si(OH)_4}$, but a dramatic effect of iron on the maximum specific growth rate (V_{max}). The modeled results from Exp-2 and Exp-3 demonstrate that the current model structure is capable of reproducing phytoplankton physiological responses to additional supply of iron by varying several key parameters used in calculating nitrate and silicate uptake. Alternatively, the potential maximum phytoplankton growth rates could be increased in the model to reflect the response to an increase of iron supply. Dugdale (1967) suggested the most likely consequence of a trace-metal limiting enzyme availability would be control over the maximum uptake rate of the affected macronutrient, e.g. NO_3. A simple model showed that increasing the concentration of the trace constituent leads to a population crash through interaction with the limiting macronutrient. Chai et al. (1996, 2000) used similar techniques but with a nitrogen-based ecosystem model to investigate iron limitation and zooplankton grazing in the equatorial Pacific. To examine the response of diatom growth to additional iron

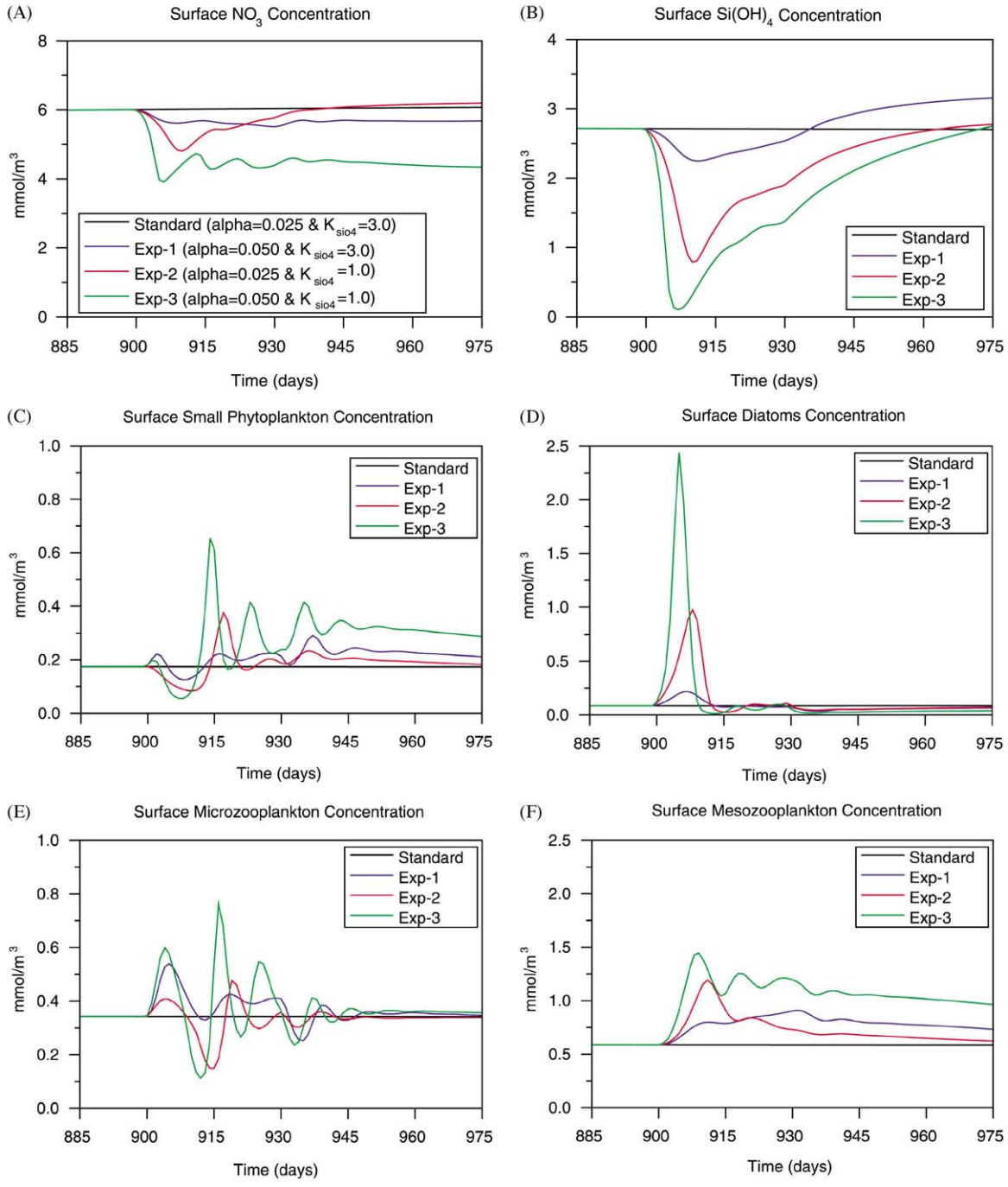

Fig. 15. Modeled surface response in three experiments. In the Exp-1, between days 900 and 930, α was increased from $0.025\,(\mathrm{W/m^2})^{-1}\,\mathrm{day}^{-1}$ (standard model run) to $0.05\,(\mathrm{W/m^2})^{-1}\,\mathrm{day}^{-1}$, and $K_{\mathrm{Si(OH)_4}}$ was unchanged (i.e., $3.0\,\mathrm{mmol\,m^{-3}}$ for the standard). In the Exp-2, during the same period, α was unchanged, but $K_{\mathrm{Si(OH)_4}}$ was decreased from $3.0\,\mathrm{mmol\,m^{-3}}$ (standard) to $1.0\,\mathrm{mmol\,m^{-3}}$. The Exp-3 was to combine experiments 1 and 2, $\alpha = 0.05\,(\mathrm{W/m^2})^{-1}\,\mathrm{day}^{-1}$ $K_{\mathrm{Si(OH)_4}} = 1.0\,\mathrm{mmol\,m^{-3}}$. Between day 900 and 930 of the model, the upwelling rate was doubled for all three experiments, which simulated an injection of iron into the euphotic zone. After 30 days at day 931 in the model, the tested parameters and upwelling rate were returned back to the values used in the standard model run.

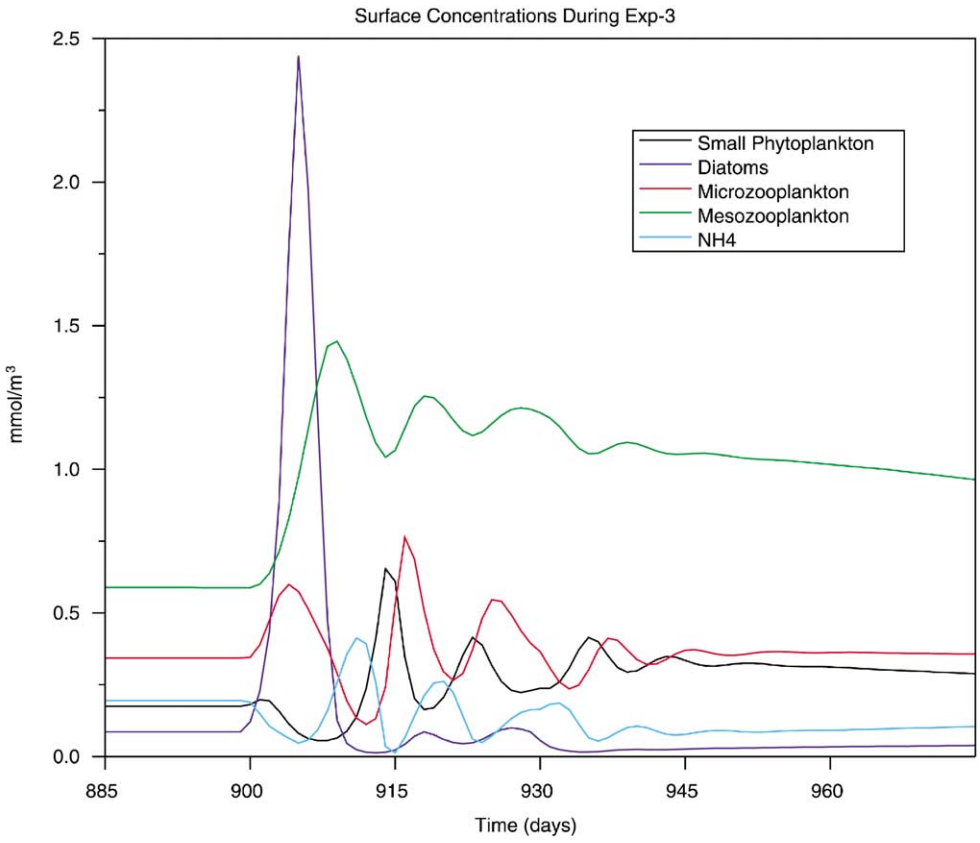

Fig. 16. Modeled surface response in the Exp-3, $\alpha = 0.05\,(\mathrm{W/m^2})^{-1}\,\mathrm{day}^{-1}$ $K_{\mathrm{Si(OH)_4}} = 1.0\,\mathrm{mmol\,m^{-3}}$. Between day 900 and 930 of the model, the upwelling rate was doubled in this experiment, which resulted in an injection of iron into the euphotic zone. After 30 days at day 931 in the model, the tested parameters and upwelling rate were returned back to the values used in the standard model run.

with the model, we have designed another model experiment, Exp-4, and compared the results between Exp-3 and Exp-4. Like three previous model experiment, in the Exp-4, between day 900 and 930 in the model, α was increased from $0.025\,(\mathrm{W/m^2})^{-1}\,\mathrm{day}^{-1}$ (standard model run) to $0.05\,(\mathrm{W/m^2})^{-1}\,\mathrm{day}^{-1}$, the upwelling rate also was doubled, $\mu 2_{\max}$, the potential maximum specific diatom growth rate, was doubled from 3.0 to $6.0\,\mathrm{day}^{-1}$. In the Exp-4, $K_{\mathrm{Si(OH)_4}}$ was unchanged (i.e., $3.0\,\mathrm{mmol\,m^{-3}}$ for the standard). After 30 days, the tested parameters and upwelling rate were returned back to the values used in the standard model run. Fig. 17 shows modeled surface diatom and silicate concentration comparison between Exp-3 and Exp-4. The increases of diatoms between these two experiments are near identical both in magnitude and temporal patterns. The modeled surface silicate concentrations are quite similar as well, except the decrease of silicate in the Exp-4 is less compared to the Exp-3. This is because the increase of diatoms in the Exp-4 is not as large as in the Exp-3, $2.0\,\mathrm{mmol\,m^{-3}}$ vs. $2.4\,\mathrm{mmol\,m^{-3}}$ for the peak values between these two experiments. Other modeled variables (not shown) are very similar between Exp-3 and Exp-4. By comparing the modeled results between Exp-3 and Exp-4, we can conclude, from the modeling point of view, that additional iron supply can either cause decreasing $K_{\mathrm{Si(OH)_4}}$ or increasing $\mu 2_{\max}$, and the modeled phytoplankton responses to the changes of these two parameters are very similar, i.e. an increase in diatom

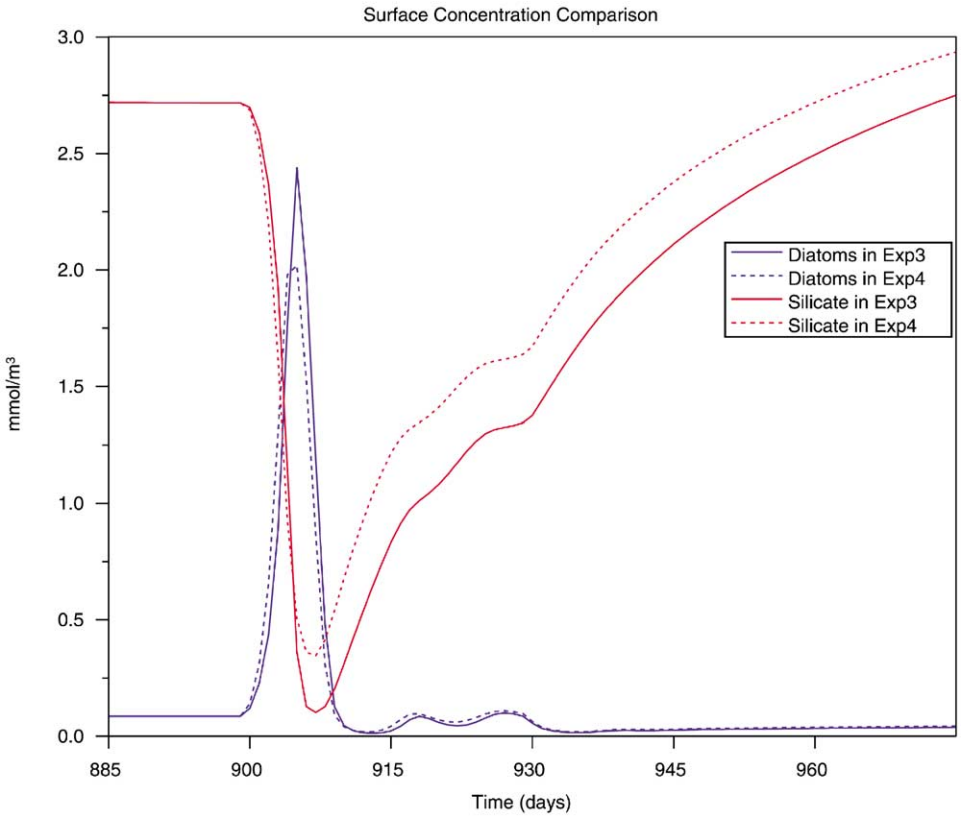

Fig. 17. Modeled surface diatom and silicate concentration comparison between Exp-3 and Exp-4. In both experiments, between day 900 and 930 in the model, α was increased from $0.025\,(\mathrm{W/m^2})^{-1}\,\mathrm{day}^{-1}$ (standard model run) to $0.05\,(\mathrm{W/m^2})^{-1}\,\mathrm{day}^{-1}$, the upwelling rate was also doubled. In the Exp-3, $K_{\mathrm{Si(OH)_4}}$ was decreased from $3.0\,\mathrm{mmol\,m^{-3}}$ (standard) to $1.0\,\mathrm{mmol\,m^{-3}}$; in the Exp-4, $K_{\mathrm{Si(OH)_4}}$ was unchanged (i.e., $3.0\,\mathrm{mmol\,m^{-3}}$ for the standard), but $\mu 2_{\max}$, the potential maximum diatom growth rate, was doubled from 3.0 to $6.0\,\mathrm{day}^{-1}$. After 30 days at day 931 in the model, the tested parameters and upwelling rate were returned back to the values used in the standard model run.

uptake of silicate. The initial slope, $V/V_{\max} = V_{\max}/K_{\mathrm{Si(OH)_4}}$, so that increasing $V_{\max}$ or decreasing $K_{\mathrm{Si(OH)_4}}$ have the same effect. There have been several reports that additional iron enhances phytoplankton specific growth rate and total phytoplankton biomass (Lindley and Barber, 1998; Boyd et al., 2000; De La Rocha et al., 2000), and the model results support such observed findings. More field studies are needed to investigate how additional iron may affect silicate uptake dynamics.

4. Conclusions

We developed a 10-component ecosystem model to address nitrogen and silicon cycle in the equatorial Pacific. The ecosystem model was forced by the area-averaged (5°S–5°N, 90°W–180°) annual mean upwelling velocity and vertical diffusivity. The model is capable of reproducing the low-silicate, high-nitrate, and low-chlorophyll (LSHNLC) conditions in the equatorial Pacific. The ecosystem model also was linked to carbon cycle through the consumption of assimilated nitrate and silicate. The results from this

modeling study are as follows:

1. The modeled vertical averaged small phytoplankton is $0.131\,\mathrm{mmol\,m^{-3}}$, and for diatoms, the value is $0.025\,\mathrm{mmol\,m^{-3}}$. The percentage of diatoms in the total modeled phytoplankton biomass is 16%, which indicates low-silicate condition, about $3.0\,\mathrm{mmol\,m^{-3}}$ near the surface, limits diatom production in the equatorial Pacific.
2. The modeled sea-to-air flux of CO_2 across the sea–air interface is $4.3\,\mathrm{mol\,m^{-2}\,yr^{-1}}$, which is consistent with the observed results ranging of 1.0–$4.5\,\mathrm{mol\,m^{-2}\,yr^{-1}}$. In order to simulate the air–sea flux of CO_2 with detailed spatial distribution and temporal variation, a complete three-dimensional simulation of the carbon cycle is needed.
3. The ammonium inhibition plays an important role in determining the nitrogen uptake dynamic in the model. The modeled surface nitrate concentration could increase by a factor of 10 (from 0.8 to $8.0\,\mathrm{mmol\,m^{-3}}$) when the strength of the ammonium inhibition increased from $\psi = 1.0$ to $10.0\,(\mathrm{mmol\,m^{-3}})^{-1}$.
4. The effects of both micro- and meso-zooplankton grazing were tested by varying the micro- and meso-zooplankton maximum grazing rates, $G1_{max}$ and $G2_{max}$. The modeled results are quite sensitive to the zooplankton grazing parameters (see Fig. 14).
5. The current model considers the role of iron implicitly through the parameters that determine the growth rate of diatoms. Several iron-enrichment experiments were conducted by changing the parameter α (the initial slope of the photosynthetic rate over irradiance at low irradiance), $K_{Si(OH)_4}$ (half-saturation concentration of silicate uptake by diatom), and $\mu 2_{max}$ (the potential maximum specific diatom growth rate) in the regulation terms of silicate uptake by diatom. Within the first 5 days in the modeled iron-enrichment experiment, the diatom biomass increased from 0.08 to $2.5\,\mathrm{mmol\,m^{-3}}$, more than a factor of 30 increase. But the diatom populations crashed 2 weeks after the experiment started, due to exhaustion of available silicate and increased mesozooplankton. The modeled iron-enrichment experiments produced several ecological behaviors similar to these observed during the IronEx-2.

Acknowledgements

F. Chai was supported by NSF Grant OCE-9802061. Two anonymous reviewers made comments that improved the final version of the manuscript. This publication is U.S. JGOFS contribution No. 695.

References

Anderson, L.A., Sarmiento, J.L., 1994. Redfield ratios of remineralization determined by nutrient data analysis. Global Biogeochemical Cycles 8, 65–80.

Bacon, M.P., Cochran, J.K., Hirschberg, D., Hammar, T.R., Fleer, A.P., 1996. Export flux of carbon at the equator during the EqPac time-series cruises estimated from ^{234}Th measurements. Deep-Sea Research II 43, 1133–1154.

Barber, R.T., Ryther, J.H., 1969. Organic chelators: factors affecting primary production in the Cromwell Current upwelling. Journal of Experimental Marine Biology and Ecology 3, 191–199.

Barber, R.T., Chavez, F.P., 1991. Regulations of primary productivity rate in the equatorial Pacific. Limnology and Oceanography 36 (8), 1803–1815.

Barber, R.T., 1992. Introduction to the WEC88 cruise: and investigation into why the equatorial is not greener. Journal of Geophysical Research 97, 609–610.

Barber, R.T., Sanderson, M.P., Lindley, S.T., Chai, F., Newton, J., Trees, C.C., Foley, D.G., Chavez, F.P., 1996. Primary productivity and its regulation in the equatorial Pacific during and following the 1991–1992 El Niño. Deep-Sea Research II 43 (4–6), 933–969.

Bidigare, R.R., Ondrusek, M.E., 1996. Spatial and temporal variability of phytoplankton pigment distributions in the central equatorial Pacific Ocean. Deep-Sea Research II 43, 809–833.

Boyd, P.W., others, 2000. A mesoscale phytoplankton bloom in the polar Southern Ocean stimulated by iron fertilization. Nature 407, 695–702.

Brzezinski, M.A., 1985. The Si:C:N ratio of marine diatoms Interspecific variability and the effect of some environmental variables. Journal of Phycology 21, 347–357.

Brzezinski, M., Phillips, D., Chavez, F., Friedrich, G., Dugdale, R., 1997. Silica production in the Monterey, California upwelling system. Limnology and Oceanography 42 (8), 1694–1705.

Busseler, K.O., Andrews, J.A., Hartman, M.C., Belastock, R., Chai, F., 1995. Regional estimates of the export flux of particulate organic carbon derived from Thorium-234 during the JGOFS EqPac program. Deep-Sea Research II 42 (2–3), 777–804.

Chai, F., Lindley, S.T., Barber, R.T., 1996. Origin and maintenance of a high NO_3 condition in the equatorial Pacific. Deep Sea Research II 43, 1031–1064.

Chai, F., Lindley, S.T., Toggweiler, J.R., Barber, R.T., 2000. Testing the importance of iron and grazing in the maintenance of the high nitrate condition in the equatorial Pacific Ocean, a physical-biological model study. In: Hanson, R.B., Ducklow, H.W., Field, J.G. (Eds.), The Changing Ocean Carbon Cycle. International Geosphere–Biosphere Programme (IGBP) Book Series 5. Cambridge University Press, Cambridge, pp. 156–186.

Chavez, F.R., Barber, R.T., 1987. An estimate of new production in the equatorial Pacific. Deep-Sea Research I 34, 1229–1243.

Chavez, F.P., Buck, K.R., Coale, K.H., Martin, J.H., DiTullio, G.R., Welshmeyer, N.A., Jacobson, A.C., Barber, R.T., 1991. Growth rates, grazing, sinking and iron limitation of equatorial Pacific phytoplankton. Limnology and Oceanography 36, 1816–1833.

Chavez, F.P., Toggweiler, J.R., 1995. Physical estimates of global new production: the upwelling contribution. In: Summerhayes, C.P., Emeis, K.-C., Angel, M.V., Smith, R.L., Zeitschel, B. (Eds.), Upwelling in the Ocean Modern Processes and Ancient Records. Wiley, New York, pp. 313–320.

Chavez, F.P., Buck, K.R., Service, S.K., Newton, J., Barber, R.T., 1996. Phytoplankton variability in the central and eastern tropical Pacific. Deep-Sea Research II 43, 835–870.

Coale, K.H., et al., 1996. A massive phytoplankton bloom induced by an ecosystem-scale iron fertilization experiment in the equatorial Pacific Ocean. Nature 838, 495–501.

Cuhel, R.L., Ortner, P.B., Lean, D.R.S., 1984. Night synthesis of protein by algae. Limnology and Oceanography 29 (4), 731–744.

Dam, H.D., Zhang, X., Butler, M., Roman, M.R., 1995. Mesozooplankton grazing and metabolism at the equator in the central Pacific: implications carbon and nitrogen fluxes. Deep-Sea Research II 42, 735–756.

De La Rocha, C.L., Brzezinski, M.A., Hutchins, D.A., Zhang, Y., 2000. Effects of iron and zinc efficiency on elemental composition and silica production of diatoms. Marine Ecology Progress Series 195, 71–79.

Dortch, Q., 1990. The interaction between ammonium and nitrate uptake in phytoplankton. Marine Ecology Progress Series 61, 138–201.

Dugdale, R.C., 1967. Nutrient limitation in the sea: dynamics, identification, and significance. Limnology and Oceanography 12 (4), 685–695.

Dugdale, R.C., Goering, J.J., 1967. Uptake of new and regenerated forms of nitrogen in primary productivity. Limnology and Oceanography 12, 196–206.

Dugdale, R.C., Wilkerson, F.P., 1998. Silicate regulation of new production in the equatorial Pacific upwelling. Nature 391, 270–273.

Dugdale, R.C., Wilkerson, F.P., Barber, R.T., Chavez, F.P., 1992. Estimating new production in the equatorial Pacific Ocean at 150°W. Journal of Geophysical Research 97, 681–686.

Dugdale, R.C., Barber, R., Chai, F., Peng, T.H., Wilkerson, F.P., 2002. One-dimensional ecosystem model of the equatorial Pacific upwelling system. Part II: sensitivity analysis and comparison with JGOFS EqPac data. Deep-Sea Research II 49, 2747–2768.

Dunne, J.P., Murray, J.W., Aufdenkampe, A.K., Blain, S., Rodier, M., 1999. Silicon–nitrogen coupling in the equatorial Pacific upwelling zone. Global Biogeochemical Cycles 13 (3), 715–726.

Eppley, R.W., Chavez, F.P., Barber, R.T., 1992. Standing stocks of particulate carbon and nitrogen in the equatorial Pacific at 150°W. Journal of Geophysical Research 97, 655–661.

Evans, G.T., Parslow, J.S., 1985. A model of annual plankton cycles. Biological Oceanography 24, 483–494.

Fasham, M.J.R., Ducklow, H.W., McKelvie, S.M., 1990. A nitrogen-based model of plankton dynamics in the oceanic mixed layer. Journal of Marine Research 48, 591–639.

Fasham, M.J.R., 1995. Variations in the seasonal cycle of biological production in subarctic oceans: a model sensitivity analysis. Deep-Sea Research I 42, 1111–1149.

Feely, R.A., Gammon, R.H., Taft, B.A., Pullen, P.E., Waterman, L.S., Conway, T.J., Gendron, J.F., Wisegarver, D.P., 1987. Distribution of chemical tracers in the eastern equatorial Pacific during and after the 1982–1983 El Niño/southern oscillation event. Journal of Geophysical Research 92, 6545–6558.

Feely, R.A., Wanninkhof, R., Goyet, C., Archer, D.E., Takahashi, T., 1997. Variability of CO_2 distributions and sea–air fluxes in the central and eastern equatorial Pacific during the 1991–1994 El Niño. Deep-Sea Research II 44 (9–10), 1851–1867.

Foley, D.G., Dickey, T.D., McPhaden, M.J., Bidigare, R.R., Lewis, M.R., Barber, R.T., Lindley, S.T., Garside, C., Manov, D.V., McNeil, J.D., 1997. Longwaves and primary productivity variations in the equatorial Pacific at 0°, 140°W. Deep-Sea Research II 44, 1801–1826.

Friedrichs, M.A.M., Hofmann, E.E., 2001. Physical control of biological processes in the central equatorial Pacific. Deep-Sea Research I 48 (4), 1023–1069.

Frost, B.W., 1987. Grazing control of phytoplankton stock in the open subarctic Pacific Ocean: a model assessing the role of mesozooplankton, particularly the large calanoid copepods, neocalanus, spp. Marine Ecology Progress Series 39, 49–68.

Frost, B.W., 1991. The role of grazing in nutrient-rich areas of the open sea. Limnology and Oceanography 36, 1616–1630.

Frost, B.W., 1996. Phytoplankton bloom on iron rations. Nature 383, 475–476.

Frost, B.W., Franzen, N.C., 1992. Grazing and iron limitation in the phytoplankton stock and nutrient concentration: a chemostat analogue of the Pacific equatorial upwelling zone. Marine Ecology Progress Series 83, 291–303.

Hofmann, E.E., Ambler, J.W., 1988. Plankton dynamics on the outer southeastern US continental shelf. Part II: a time-dependent model. Journal of Marine Research 9, 235–248.

Hutchins, D.A., Bruland, K.W., 1998. Iron-limited diatom growth and Si:N uptake rations in a coastal upwelling regime. Nature 393, 561–564.

Inoue, H., Sugimura, Y., 1992. Variations and distributions of CO_2 in and over the equatorial Pacific during the period from 1986/88 El Niño event to the 1988/89 La Niña event. Tellus 44B, 1–22.

Jamart, B.M., Winter, D.F., Banse, K., Anderson, G.C., Lam, R.K., 1977. A theoretical study of phytoplankton growth and nutrient distribution in the Pacific Ocean of the northwestern US coast. Deep-Sea Research 24, 753–773.

Keeling, C.D., Revelle, R., 1985. Effects of El Niño/Southern Oscillation on the atmospheric content of carbon dioxide. Meteoritics 20, 437–450.

Ku, T.L., Luo, S., Kusakabe, M., Bishop, J.K.B., 1995. ^{228}Ra-derived nutrient budgets in the upper equatorial Pacific and the role of "new" silicate in limiting productivity. Deep-Sea Research II 42, 479–497.

Landry, M.R., Constantinou, J., Kirshtein, J., 1995. Microzooplankton grazing in the central equatorial Pacific during February and August, 1992. Deep-Sea Research II 42, 657–672.

Landry, M.R., Barber, R.T., Bidigare, R.R., Chai, F., Coale, K.H., Dam, H.G., Lewis, M.R., Lindley, S.T., McCarthy, J.J., Roman, M.R., Stoecker, D.K., Verity, P.G., White, J.R., 1997. Iron and grazing constraints on primary production in the central equatorial Pacific: an EqPac synthesis. Limnology and Oceanography 42, 405–418.

Leonard, C.L., McClain, C.R., Murtugudde, R., Hofmann, E.E., Harding Jr., L.W., 1999. An iron-based ecosystem model of the central equatorial Pacific. Journal of Geophysical Research 104, 1325–1341.

Leynaert, A., Treguer, P., Lancelot, C., Rodier, M., 2001. Silicon limitation of biogenic silica production in the equatorial Pacific. Deep-Sea Research I 48, 639–660.

Levitus, S., Reid, J.L., Conkright, M.E., Najjar, R., 1993. Distribution of nitrate, phosphate and silicate in the world ocean. Progress in Oceanography 31, 245–273.

Lindley, S.T., Barber, R.T., 1998. Phytoplankton response to natural and experimental iron addition. Deep-Sea Research II 45, 1135–1150.

Lindley, S.T., Bidigare, R.R., Barber, R.T., 1995. Phytoplankton photosynthesis parameters along 140W in the equatorial Pacific. Deep-Sea Research II 42, 441–464.

Loukos, H., Frost, B., Harrison, D.E., Murray, J.W., 1997. An ecosystem model with iron limitation of primary production in the equatorial Pacific at 14°W. Deep Sea Research II 44, 2221–2249.

Martin, J.H., IronEx team, 1994. Testing the iron hypothesis in ecosystems of the equatorial Pacific Ocean. *Nature* 371, 123–129.

McCarthy, J.J., Garside, C., Nevins, J.L., Barber, R.T., 1996. New production along 140°W in the equatorial Pacific during and following the 1992 El Niño event. Deep-Sea Research II 43, 1065–1093.

Millero, F.J., Lee, K., Roche, M., 1998. Distribution of alkalinity in the surface waters of the major oceans. Marine Chemistry 60, 111–130.

Minas, H.J., Minas, M., 1992. Net community production in "high nutrient-low chlorophyll" waters of the tropical and Antarctic Oceans: grazing versus iron hypothesis. Oceanologia Acta 15, 145–162.

Minas, H.J., Minas, M., Packard, T.T., 1986. Productivity in upwelling areas deduced from hydrographic and chemical fields. Limnology and Oceanography 31, 1182–1206.

Monger, B., et al., 1997. Frequency response of a simple food chain model with time-delayed recruitment: implications for abiotic–biotic coupling. In: Tuljapurkar, S., Caswell, H. (Eds.), Structured Population Models in Marine, Terrestrial and Freshwater Systems. Chapman & Hall, New York.

Murray, J.M., Barber, R.T., Bacon, M.P., Roman, M.R., Feely, R.A., 1994. Physical and biological controls on carbon cycling in the equatorial Pacific. Science 266, 58–65.

Murray, J.W., Johnson, E., Garside, C., 1995. A U.S. JGOFS process study in the equatorial Pacific (EqPac): introduction. Deep Sea Research II 42, 275–293.

Murray, J.W., Young, J., Newton, J., Dunne, J., Chapin, T., Paul, B., McCarthy, J.J., 1996. Export flux of particulate organic carbon from the central equatorial Pacific determined using a combined drifting trap—^{234}Th approach. Deep Sea Research II 43, 1095–1133.

Nelson, D.M., Treguer, P., 1992. Role of silicon as a limiting nutrient to Antarctic diatoms: evidence from kinetic studies in the Ross Sea ice-edge zone. Marine Ecology Progress Series 80, 255–264.

Nelson, D.M., Goering, J.J., Boisseau, D.W., 1981. Consumption and regeneration of silicic acid in three upwelling systems. In: Richards, F.A. (Ed.), Coastal Upwelling. American Geophysical Union, pp. 242–256.

Nelson, D.M., Treguer, P., Brzezinski, M.A., Leynaert, A., Queguiner, B., 1995. Production and dissolution of biogenic silica in the ocean: revised global estimates, comparison with regional data and relationship to biogenic sedimentation. Global Biogeochemical Cycles 9 (3), 359–372.

Pacanowski, R.C., Philander, S.G.H., 1981. Parameterization of vertical mixing in numerical models of tropical oceans. Journal of Physical Oceanography 11, 1443–1451.

Peinert, R., et al., 1989. Food web structure and loss rate. In: Berger, W.H., Smetacek, V.S., Wefer, G. (Eds.), Productivity of the Ocean; Present and past. Dahlem Workshop Reports, Vol. 44, pp. 35–48.

Peña, M.A., Lewis, M.R., Harrison, W.G., 1990. Primary productivity and size structure of phytoplankton biomass on a transect of the equator at 135°W in the Pacific Ocean. Deep-Sea Research 37, 295–315.

Price, N.M., Ahner, B.A., Morel, F.M.M., 1994. The equatorial Pacific Ocean: grazer controlled phytoplankton populations in an iron-limited ecosystem. Limnology and Oceanography 39, 520–534.

Roman, M.R., Gauzens, A.L., 1997. Copepod grazing in the equatorial Pacific. Limnology and Oceanography 42 (4), 623–634.

Sarmiento, J.L., Slater, R.D., Fasham, M.J.R., Ducklow, H.W., Toggweiler, J.R., Evans, G.T., 1993. A seasonal three-dimensional ecosystem model of nitrogen cycling in the North Atlantic euphotic zone. Global Biogeochemical Cycles 7, 417–450.

Smetacek, V., 1985. The annual cycle of Kiel bight plankton—a long term analysis. Estuaries 8, 145–157.

Smethie Jr., W.M., Takahashi, T., Chipman, D.W., Ledwell, J.R., 1985. Gas exchange and CO2 flux in the Atlantic including Rn and *p*CO2 measurements. Journal of Geophysical Research 90, 7005–7022.

Takahashi, T., Goddard, J., Southerlabd, S., Chipman, D.W., Breeze, C.C., 1986. Seasonal and geographic variability of carbon dioxide sink/source in the ocean areas. Technical Report, contract MERTTA 19X.89675C, 66pp, Lamont-Doherty Geol. Obs., Palisades, NY.

Takeda, S., 1998. Influence of iron availability on nutrient consumption ratio of diatoms in oceanic waters. Nature 393, 774–776.

Thomas, W.H., 1972. Nutrient inversions in the southeastern tropical Pacific Ocean. Fishery Bulletin 70, 929–932.

Toggweiler, J.R., Carson, S., 1995. What are upwelling systems contributing to the ocean's carbon and nutrient budgets? In: Summerhayes, C.P., Emeis, K.-C., Angel, M.V., Smith, R.L., Zeitzschel, B. (Eds.), Upwelling in the Ocean: Modern Processes and Ancient Records. Wiley, New York, pp. 337–360.

Verity, P.G., Stoecker, D.K., Sieracki, M.E., Nelson, J.R., 1996. Microzooplankton grazing of primary production at 140W in the equatorial Pacific. Deep-Sea Research II 43, 1227–1256.

Volk, T., 1989. Effect of the equatorial Pacific upwelling on atmospheric CO2 during the 1982–83 El Niño. Global Biogeochemical Cycles 3, 267–279.

Walsh, J.J., 1976. Herbivory as a factor in patterns of nutrient utilization in the sea. Limnology and Oceanography 21, 1–13.

Wanninkhof, R., Feely, R.A., Atwood, D.K., Berberian, G., Wilson, D., Murphy, P.P., Lamb, M.F., 1995. Seasonal and lateral variations in carbon chemistry of surface water in the eastern equatorial Pacific during 1992. Deep-Sea Research II 42, 387–410.

Wefer, G., 1989. Particle flux in the ocean: effects of episodic production. In: Berger, W.H., Smetacek, V.S., Wefer, G. (Eds.), Productivity of the Ocean; Present and Past. Dahlem Workshop Reports, Vol. 44, pp. 85–98.

Wheeler, P.A., Kokkinakis, S.A., 1990. Ammonium limits nitrate use in the oceanic subarctic Pacific. Limnology and Oceanography, 35, 1267–1278.

Wong, C.S., Chan, Y.H., Page, J.S., Smith, G.E., Bellegay, R.D., 1993. Changes in equatorial CO2 flux and new production estimated from CO2 and nutrient levels in Pacific surface waters during the 1986–87 El Niño. Tellus 45B, 64–79.

Wroblewski, J., 1977. A simulation of the distribution of Acartia clausii during Oregon upwelling August 1973. Journal of Plankton Research 2, 43–68.

Wyrtki, K., 1981. An estimate of equatorial upwelling in the Pacific. Journal of Physical Oceanography, 11, 1205–1214.

Zhang, X., Dam, H.D., White, J.R., Roman, M.R., 1995. Latitudinal variations in mesozooplankton grazing and metabolism in the central tropical Pacific during the U.S. JGOFS EqPac study. Deep-Sea Research II 42, 695–714.